EC Journals.ASM.org

The *Aspergillus fumigatus sitA* Phosphatase Homologue Is Important for Adhesion, Cell Wall Integrity, Biofilm Formation, and Virulence

Vinícius Leite Pedro Bom,[a] Patrícia Alves de Castro,[a] Lizziane K. Winkelströter,[a] Marçal Marine,[a] Juliana I. Hori,[a] Leandra Naira Zambelli Ramalho,[b] Thaila Fernanda dos Reis,[a] Maria Helena S. Goldman,[c] Neil Andrew Brown,[a] Ranjith Rajendran,[d] Gordon Ramage,[d] Louise A. Walker,[e] Carol A. Munro,[e] Marina Campos Rocha,[f] Iran Malavazi,[f] Daisuke Hagiwara,[g] Gustavo H. Goldman[a,h]

Faculdade de Ciências Farmacêuticas de Ribeirão Preto,[a] Faculdade de Medicina de Ribeirão Preto,[b] and Faculdade de Filosofia, Ciências e Letras de Ribeirão Preto,[c] Universidade de São Paulo, Ribeirão Preto, Brazil; Infection and Immunity Research Group, Glasgow Dental School, School of Medicine, College of Medical, Veterinary and Life Sciences, The University of Glasgow, Glasgow, United Kingdom[d]; School of Medical Sciences, University of Aberdeen, Aberdeen, United Kingdom[e]; Departamento de Genética e Evolução, Centro de Ciências Biológicas e da Saúde, Universidade Federal de São Carlos, São Paulo, Brazil[f]; Medical Mycology Research Center, Chiba University, Chiba, Japan[g]; National Laboratory of Science and Technology of Bioethanol (CTBE), Campinas, Brazil[h]

***Aspergillus fumigatus* is an opportunistic pathogenic fungus able to infect immunocompromised patients, eventually causing disseminated infections that are difficult to control and lead to high mortality rates. It is important to understand how the signaling pathways that regulate these factors involved in virulence are orchestrated. Protein phosphatases are central to numerous signal transduction pathways. Here, we characterize the *A. fumigatus* protein phosphatase 2A SitA, the *Saccharomyces cerevisiae* Sit4p homologue. The *sitA* gene is not an essential gene, and we were able to construct an *A. fumigatus* null mutant. The Δ*sitA* strain had decreased MpkA phosphorylation levels, was more sensitive to cell wall-damaging agents, had increased β-(1,3)-glucan and chitin, was impaired in biofilm formation, and had decreased protein kinase C activity. The Δ*sitA* strain is more sensitive to several metals and ions, such as $MnCl_2$, $CaCl_2$, and LiCl, but it is more resistant to $ZnSO_4$. The Δ*sitA* strain was avirulent in a murine model of invasive pulmonary aspergillosis and induces an augmented tumor necrosis factor alpha (TNF-α) response in mouse macrophages. These results stress the importance of *A. fumigatus* SitA as a possible modulator of PkcA/MpkA activity and its involvement in the cell wall integrity pathway.**

Human opportunistic pathogenic fungi are able to infect immunocompromised patients, causing disseminated infections that are difficult to control. Among fungal human infections, invasive aspergillosis (IA) has one of the highest mortality rates. Immunocompromised patients can acquire IA through the inhalation of conidia that invade the pulmonary alveoli, translocating into the blood and subsequently disseminating to other organs and niches throughout the human body. *Aspergillus fumigatus* is the main causal agent of aspergillosis (1, 2), causing around 65% of all *Aspergillus* invasive infections, and is the most encountered species in pulmonary infections (3–5). Aspergillosis is a multifactorial disease, with several phenotypes influencing the final outcome of the disease. Recent advances have revealed several key pathogenicity determinants involved in the establishment of infection, such as the composition of the cell wall, iron assimilation, hypoxia tolerance, gliotoxin production, and thermophily (1). However, it is important to understand how these traits are orchestrated and the signaling pathways that regulate them during virulence. *A. fumigatus* is able to alter its metabolism, secretome, and cell surface in order to adapt to the distinct microenvironments encountered within the host, while also being able to bypass host defenses. Consequently, it is very important to understand the signaling pathways and molecular mechanisms that are involved in virulence, as this will provide new insights into the pathosystem and the development of new approaches to combat the diverse range of diseases caused by this deadly pathogen.

The protein phosphorylation state regulates protein activity, localization, and function (6), with protein phosphorelays performing a crucial role in signal transduction. Thus, protein kinases and phosphatases perform opposing functions in numerous signal transduction cascades. Mitogen-activated protein kinase (MAPK) phosphorylation cascades are important for relaying, integrating, and amplifying intracellular signals and are crucial signaling components involved in many cellular processes (7). In *Saccharomyces cerevisiae*, MAP kinases control mating, the cellular response to high environmental osmolarity, pseudohyphal development, sporulation of diploid cells, and the maintenance of cell wall integrity in response to stresses, such as heat stress and low osmolarity (8). For instance, the *S. cerevisiae* cell wall integrity (CWI) pathway is activated when Pkc1p phosphorylates Bck1p, a mitogen-activated protein kinase kinase kinase (MAPKKK) that functions via the sequential phosphorylation of two other protein kinases (MAPKK and MAPK), resulting in the activation of a multifunctional MAP kinase (8). *S. cerevisiae* MAPKKs, Mkk1p and Mkk2p, phosphorylate the MAPK Slt2p. Mkk1p/Mkk2p and Slt2p

Received 22 January 2015 **Accepted** 9 April 2015

Accepted manuscript posted online 24 April 2015

Citation Bom VLP, de Castro PA, Winkelströter LK, Marine M, Hori JI, Ramalho LNZ, dos Reis TF, Goldman MHS, Brown NA, Rajendran R, Ramage G, Walker LA, Munro CA, Rocha MC, Malavazi I, Hagiwara D, Goldman GH. 2015. The *Aspergillus fumigatus sitA* phosphatase homologue is important for adhesion, cell wall integrity, biofilm formation, and virulence. Eukaryot Cell 14:728–744. doi:10.1128/EC.00008-15.

Address correspondence to Gustavo H. Goldman, ggoldman@usp.br.

Supplemental material for this article may be found at http://dx.doi.org/10.1128/EC.00008-15.

Copyright © 2015, American Society for Microbiology. All Rights Reserved.

doi:10.1128/EC.00008-15

regulate the expression of many downstream protein targets, such as cell wall proteins and enzymes involved in cell wall biogenesis (9).

In filamentous fungi, the conserved MAPK pheromone response, filamentous growth, osmotic-stress response, and cell wall integrity pathways have been shown to influence numerous virulence traits, including invasive growth, biofilm formation, mycotoxin production, and antifungal tolerance (8, 10–14). *A. fumigatus* has four MAPKs, MpkA (regulation of cell wall integrity signaling and pyomelanin formation), MpkB (mating and putative pheromone signaling), MpkC (regulation of conidial germination), and SakA (the Hog1 orthologue, which is involved in osmotic stress, carbon and nitrogen starvation, and regulation of conidial germination) (15–20). The *A. fumigatus* CWI pathway is composed of three MAP kinases designated Bck1, Mkk2, and MpkA. Deletion of the genes encoding these three kinases resulted in mutants with increased sensitivity to cell wall-damaging agents and morphological alterations (18, 19, 21, 22). The *A. fumigatus* CWI pathway was further characterized by the identification of putative CWI stress sensors, Wsc1, Wsc3, and MidA; the Rho GTPase Rho1; and Rom2, a guanine nucleotide exchange factor (23). Rom2 has been positioned between Wsc1, Wsc3, MidA, and Rho1 and their downstream effector MAP kinase module Bck1-Mkk2-MpkA (24).

S. cerevisiae phosphatases, such as Msg5p and Sdp1p, dephosphorylate Mpk1, contributing to the regulation of this signal transduction pathway (25). Angeles de la Torre-Ruiz et al. (26) have reported that the correct downregulation of both basal and induced activities of the protein kinase C1 (PKC1)-MAPK pathway require the function of the Sit4p phosphatase. Sit4p is a type 2A-related serine-threonine phosphatase that functions in the G_1/S transition of the mitotic cycle and is a nuclear protein that modulates functions mediated by Pkc1p, including cell wall and actin cytoskeleton organization (26–29). The protein kinase TOR (target of rapamycin) promotes the phosphorylation of Sit4p by negatively regulating Sit4p through its association with Tap42p. If TOR is inactivated by rapamycin treatment or nitrogen starvation, downstream effectors of TOR are dephosphorylated in a Sit4p-dependent manner (30). Recently, aiming to comprehend the functions of protein phosphatases in *A. fumigatus*, we identified 32 phosphatase catalytic-subunit-encoding genes (31). Within this phosphatase null mutant collection was the *sitA* deletion strain, representing the *S. cerevisiae* Sit4p homologue. Here we show that the Δ*sitA* strain has decreased MpkA phosphorylation, is more sensitive to cell wall-damaging agents, has increased β-(1,3)-glucan and chitin and reduced protein kinase C activity, and is impaired in biofilm formation, while also being avirulent in a murine model of invasive pulmonary aspergillosis. These results stress the importance of the *A. fumigatus* SitA phosphatase as a possible modulator of PkcA/MpkA activity and virulence.

MATERIALS AND METHODS

Ethics statement. The principles that guide our studies are based on the Declaration of Animal Rights ratified by UNESCO on 27 January 1978 in its 8th and 14th articles. All protocols used in this study were approved by the local ethics committee for animal experiments from the Campus of Ribeirão Preto, Universidade de São Paulo (permit number 08.1.1277.53.6; Studies on the Interaction of *Aspergillus fumigatus* with Animals). All animals were housed in groups of five within individually ventilated cages and were cared for in strict accordance with the principles outlined by the Brazilian College of Animal Experimentation (Princípios Éticos na Experimentação Animal—Colégio Brasileiro de Experimentação Animal [COBEA]) and the Guiding Principles for Research Involving Animals and Human Beings of the American Physiological Society. All efforts were made to minimize suffering. The animals were clinically monitored at least twice daily and humanely sacrificed if moribund (defined as lethargy, dyspnea, hypothermia, and weight loss). All stressed animals were sacrificed by cervical dislocation.

Strains and media. The *A. fumigatus* parental strains used in this study were CEA17 (*pyrG*$^-$) and CEA17-80. The *A. fumigatus* mutants constructed in this study were Δ*sitA* and Δ*sitA*::*sitA*$^+$. Media were of two basic types: a complete medium with three variants—YAG (2% glucose, 0.5% yeast extract, 2% agar, trace elements), YUU (YAG supplemented with 1.2 g/liter each uracil and uridine), and liquid YG or YUU medium of the same composition, but without agar—and a modified minimal medium (MM) (1% glucose, original high-nitrate salts, trace elements, 2% agar, pH 6.5) that was also used. The trace elements, vitamins, and nitrate salts were described previously (32).

DNA manipulations and construction of the *A. fumigatus* mutants. The cassettes for gene replacement were constructed by *in vivo* recombination in *S. cerevisiae* as previously described (33). Approximately 1.5 kb from the 5′ untranslated region (UTR) and the 3′ UTR flanking region of the targeted genes was selected for primer design. The primers 5F and 3R contained a short sequence homologous to the multiple cloning site (MCS) of the pRS426 plasmid. Both the 5′ and 3′ UTR fragments were PCR amplified from *A. fumigatus* genomic DNA (gDNA). The *pyrG* gene inserted into the gene replacement cassettes was amplified from the pCDA21 plasmid and was used to generate a marker for prototrophy in the mutant strains. Each fragment, along with the BamHI/EcoRI-cut pRS426 plasmid, was transformed into the *S. cerevisiae* strain SC9721 using the lithium acetate method (34). The transformant DNA was extracted according to the method of Winkelströter et al. (31). The cassette was PCR amplified from the plasmids utilizing TaKaRa *Ex Taq* DNA polymerase (Clontech TaKaRa Bio) and used for *A. fumigatus* transformation. Southern blotting was performed as described previously (35), aiming to demonstrate that the transformation cassettes had integrated homologously at the targeted *A. fumigatus* loci. DNA fragments were labeled with [α-^{32}P]dCTP using the RTS Rad Prime DNA-labeling system kit (Invitrogen).

A spontaneous *pyrG* mutant was selected from the deletion mutant strain by using fluoorotic acid, and the mutant was complemented by cotransforming the pCDA21 vector containing the *A. fumigatus pyrG* gene plus the wild-type *sitA* gene and selecting for uracil and uridine prototrophy. The primers mentioned above are described in Table S1 in the supplemental material. All the Southern blots and PCRs and the corresponding strategies to evaluate if the phosphatase genes were deleted are shown in Fig. S1 in the supplemental material.

Phenotypic assays. The phenotypes of the deletion mutants were evaluated either by radial growth or by assessing the initial growth of a droplet of conidia from a serial dilution at different temperatures in the presence or absence of oxidative and osmotic stressing agents plus reagents that cause cell wall or DNA damage. Dropout experiments were performed using 5 μl of a 10-fold dilution series starting at a concentration of 2×10^7 for the wild-type and mutant strains spotted on different growth media and grown for 48 h at 37°C.

Fungal adhesion and biofilm formation assays. The *A. fumigatus* crystal violet (CV) assay and biofilm growth assays were performed according to the methods of Mowat et al. and Shopova et al. (36, 37), respectively. In order to determine the ability to form biofilms, 1×10^4 conidia were inoculated into 200 μl MM or YG liquid medium in a 96-well polystyrene microtiter plate, which was incubated, without agitation, at 37°C for 24 h. Subsequently, the plate was washed exhaustively with phosphate-buffered saline (PBS) prior to incubation with 200 μl 0.5% crystal violet solution for 5 min at room temperature. The stained mycelia

were then exhaustively washed with sterile water and air dried. Finally, the crystal violet was eluted from the wells using 100% ethanol, and the absorbance was measured at 590 nm.

For biofilm formation, asexual spore suspensions (10^6 spores in total) were added to 20 ml HEPES-buffered RPMI 1640 with L-glutamine (Life Technologies) and dispensed on flat, presterilized polystyrene petri dishes. Following an initial adherence phase of 4 h during static incubation in RPMI at 37°C, unbound conidia were washed three times with sterile PBS-0.1% Tween 80 solution (PBS composition: NaCl, 137 mM; KCl, 2.7 mM; Na_2HPO_4, 10 mM; and KH_2PO_4, 1.8 mM). Fresh RPMI medium with the indicated additives was added to the adhered conidia, and static submerged cultures were grown for up to 96 h at 37°C. Mycelia were harvested by scraping from the surfaces of the petri dishes and filtered through Miracloth (Merck). The dry weight of biofilm produced was determined.

Scanning electron microscopy (SEM). Standardized conidia of the Δ*sitA* strain and its parental strain were inoculated in RPMI medium onto Thermanox coverslips (13 mm) in a 24-well tissue culture plate. After 24 h of incubation at 37°C, the biofilms were processed and imaged as previously described (38). Briefly, the biofilms were washed in PBS and fixed in 2% paraformaldehyde, 2% glutaraldehyde, and 0.15% (wt/vol) alcian blue in 0.15 M sodium cacodylate (pH 7.4). The biofilms were sputter coated with gold and viewed under a JEOL JSM-6400 scanning electron microscope in high-vacuum mode at 10 kV.

Transmission electron microscopy (TEM). Preparation of samples was as previously described (39) with the following modifications. Briefly, cells were collected, and the pellets were fixed with 2.5% (vol/vol) glutaraldehyde in 0.1 M sodium phosphate buffer (pH 7.3) for 24 h at 4°C. Samples were encapsulated in 3% (wt/vol) low-melting-point agarose prior to processing to Spurr resin following a 24-h schedule on a Lynx tissue processor (secondary 1% OsO_4 fixation, 1% uranyl acetate contrasting, ethanol dehydration, and infiltration with acetone/Spurr resin). Additional infiltration was provided under vacuum at 60°C before embedding in capsules (TAAB Laboratory and Microscopy, United Kingdom) and polymerizing at 60°C for 48 h. Semithin (0.5-μm) survey sections were stained with toluidine blue to identify the areas of best cell density. Ultrathin sections (60 nm) were prepared using a Diatome diamond knife on a Leica UC6 ultramicrotome and stained with uranyl acetate and lead citrate for examination with a JEM-1400Plus transmission electron microscope (JEOL [United Kingdom] Ltd., Hertfordshire, United Kingdom) and imaging with an AMT UltraVue camera and AMT Image Capture Engine V602 software (Deben United Kingdom Ltd., Suffolk, United Kingdom).

Staining for dectin-1 and chitin. Staining for dectin-1 and chitin was performed as described previously (31, 40). Briefly, *A. fumigatus* conidia were grown for 6 h at 37°C, UV irradiated, blocked using blocking solution (2% goat serum, 1% bovine serum albumin [BSA], 0.1% Triton X-100, 0.05% Tween 20, 0.05% sodium azide, and 0.01 M PBS) for 1 h at room temperature, and stained with conditioned medium containing 1 μg/ml of soluble human dectin-1a fused to an IgG1 Fc domain (s-dectin-hFc; InvivoGen, San Diego, CA), followed by DyLight 594-conjugated goat anti-human IgG1 (41). For chitin staining, UV-irradiated germlings were treated with 2 μg/ml calcofluor white (CFW) for 5 min. After washing, the stained cells were visualized under identical imaging conditions for parallel comparison using a Zeiss Observer Z1 fluorescence microscope. Staining was quantified as the amount of staining averaged to the total fungal area using ImageJ software.

Analysis of conidial surface proteins. Total proteins from the fungal conidial surface were extracted as described previously (42). Briefly, 2×10^9 conidia from three independent samples of the wild-type and Δ*sitA* strains were incubated with 200 μl of 0.5 M NaCl solution for 2 h at room temperature. The supernatant was collected by centrifugation at 12,000 rpm for 5 min, lyophilized, and resuspended in 50 μl of buffer (0.1 M Tris-HCl, pH 8.8, with 8 M urea). The proteins were quantified using the Bradford method with protein assay dye reagent concentrate (Bio-Rad; catalog no. 500-0006, lot L9700067 Rev J). The sample preparation for mass spectrometry consisted of three main steps. (i) Protein reduction and alkylation were performed by adding 2.5 μl of dithiotreitol (DTT) at a ratio of 1 mg DTT/mg protein and incubation for 2 h at room temperature, followed by alkylation by adding 5 μl of iodoacetamide at a ratio of 3 mg iodoacetamide/mg protein and incubation for 1 h at room temperature. (ii) Enzymatic digestion of the proteins was done with trypsin. The sample was diluted 5-fold in 0.1 M ammonium bicarbonate, pH ≥8.0, yielding a final volume of 300 μl. The samples were then incubated with 1 μg of trypsin (Promega; V511A, lot 30551310) at 37°C for 16 h. (iii) Cleanup and desalting of the samples were done using the column Oasis HLB Cartridge 1cc (catalog number 186000383; Waters). The column was equilibrated with a solution containing 5% acetonitrile, 0.1% formic acid, and the elution of the material was performed with 80% acetonitrile. The samples were dried and applied to an LTQ Orbitrap Elite mass spectrometer (Thermo-Finnigan) coupled to a nanoflow chromatography system (liquid chromatography-tandem mass spectrometry [LC–MS-MS]). The acquired data were automatically processed with the Computational Proteomics Analysis System (CPAS) (43). The identified peptides were grouped into proteins using the algorithm Protein Prophet, and a list of identified proteins was established using an error lower than 2%. The data were compared with *A. fumigatus* proteomes (Af293 or A1163) at http://www.aspgd.org.

Murine model of pulmonary aspergillosis. The murine model of pulmonary aspergillosis was performed according to the method of Dinamarco et al. (44). Outbreed female mice (BALB/c strain; body weight, 20 to 22 g) were housed in vented cages containing 5 animals. The mice were immunosuppressed with cyclophosphamide at a concentration of 150 mg per kg of body weight, which was administered intraperitoneally on days −4 and −1 prior to infection (day 0) and day 2 postinfection. Hydrocortisone acetate (200 mg/kg) was injected subcutaneously on day −3. The *A. fumigatus* conidia used for inoculation were grown on *Aspergillus* complete YAG for 2 days prior to infection. Fresh conidia were harvested in PBS and filtered through a Miracloth (Calbiochem). The conidial suspensions were spun for 5 min at 3,000 × *g*, washed three times with PBS, counted using a hemocytometer, and then resuspended at a concentration of 5.0×10^6 conidia/ml. Viability counts for the administered inoculum were determined following serial dilution and plating on *Aspergillus* YAG, and the conidia were grown at 37°C. The mice were anesthetized by halothane inhalation and infected by intranasal instillation of 1.0×10^5 conidia in 20 μl of PBS. As a negative control, a group of 5 mice received PBS only. The mice were weighed every 24 h from the day of infection and visually inspected twice daily. In the majority of cases, the endpoint for survival experimentation was identified when a 20% reduction in body weight was recorded, at which time the mice were sacrificed. The statistical significance of comparative survival values was calculated using log rank analysis with the Prism statistical analysis package. Additionally, at 3 days postinfection, 2 mice per strain were sacrificed, and the lungs were removed, fixed, and processed for histological analysis.

Lung histopathology and fungal burden. After sacrifice, the lungs of the mice were removed and fixed for 24 h in 3.7% formaldehyde-PBS. Samples were washed several times in 70% alcohol before dehydration in a series of alcohol solutions at increasing concentrations. Finally, the samples were incubated in xylol and embedded in paraffin. For each sample, sequential 5-μm-thick sections were collected on glass slides and stained with Gomori methenamine silver (GMS) or hematoxylin and eosin (HE) stain following standard protocols (2). Briefly, the sections were deparaffinized, oxidized with 4% chromic acid, stained with methenamine silver solution, and counterstained with hematoxylin. Tissue sections were also stained with hematoxylin and eosin for histological examination to determine lung damage. All the stained slides were immediately washed, preserved in mounting medium, and sealed with a coverslip. Microscopic analyses were performed using an Axioplan 2 imaging microscope (Carl Zeiss) at the stated magnifications under bright-field conditions.

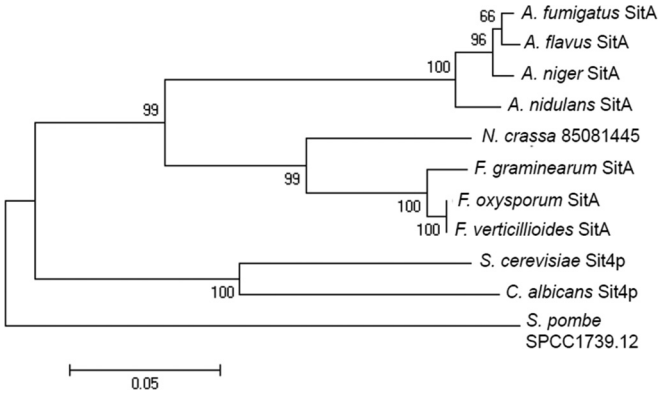

FIG 1 Phylogenetic tree of the fungal SitA homologues. The optimal tree for the *A. fumigatus* and *S. cerevisiae* phosphatases is shown. The tree was inferred using the neighbor-joining method. The bootstrap values calculated for 500 replicates are indicated on the tree branches. The sequences were aligned with ClustalW, and the tree was constructed by using MEGA6 software. *F. verticillioides*, *Fusarium verticillioides*; *F. oxysporum*, *Fusarium oxysporum*; *A. flavus*, *Aspergillus flavus*; *A. nidulans*, *Aspergillus nidulans*; *N. crassa*, *Neurospora crassa*; *S. pombe*, *Schizosaccharomyces pombe*.

To investigate fungal burdens in the lungs, mice were infected as described in the previous paragraph but with a higher inoculum of 1×10^6 conidia/20 μl. A higher inoculum than in the survival experiments was used to increase fungal DNA detection. Animals were sacrificed 72 h postinfection, and both lungs were harvested and immediately frozen in liquid nitrogen. Samples were homogenized by vortexing with glass beads for 10 min, and DNA was extracted via the phenol-chloroform method. The DNA quantity and quality were assessed using a NanoDrop 2000 spectrophotometer (Thermo Scientific). At least 300 to 500 ng of total DNA from each sample was used for quantitative real-time PCRs. A primer and a Lux probe (Invitrogen) were used to amplify the 18S rRNA region of *A. fumigatus* (primer, 5′-CTTAAATAGCCCGGTCCGCATT-3′; probe, 5′-CATCACAGACCTGTTATTGCCG-3′) and an intronic region of mouse GAPDH (glyceraldehyde-3-phosphate dehydrogenase) (primer, 5′-CGAGGGACTTGGAGGACACAG-3′; probe, 5′-GGGCAA GGCTAAAGGTCAGCG-3′). Six-point standard curves were calculated using serial dilutions of gDNA from all the *A. fumigatus* strains used and the uninfected mouse lung. Fungal and mouse DNA quantities were obtained from the threshold cycle (C_T) values from an appropriate standard curve. The fungal burden was determined as the ratio between picograms of fungal and micrograms of mouse DNA.

Phagocytosis index. Alveolar macrophages (AMs) were obtained from the lungs of of BALB/c mice (8 to 10 weeks old) by bronchoalveolar lavage (BAL) with 1 ml of RPMI 1640 medium (Sigma-Aldrich) using an intravenous catheter (Becton Dickinson) and pumping the medium into the lungs through the trachea. Six mice per experiment were sacrificed. Macrophages from all six animals were mixed and centrifuged at 4,000 rpm for 5 min. The supernatant was removed, and the pellet was washed with 5 ml of RPMI and resuspended in 1 ml of RPMI-10% fetal bovine serum (FBS) (Gibco). The AMs were counted in a hemocytometer. The phagocytic assay was performed according to the methods of Dinamarco et al. and Mech et al. (44, 45), with some changes. Briefly, in a 24-well plate containing one 15-mm-diameter coverslip per well, about 2×10^4 macrophages were incubated with 1 ml of RPMI-FBS at 37°C with 5% CO_2 for 1 h. Afterward, the wells were washed with 1 ml of assay medium to remove nonadherent cells. Alveolar macrophages are adherent, and following this step, the number of macrophages obtained is typically greater than 90%. To each well, 1 ml of RPMI-FBS containing 1×10^5 conidia (1:5 macrophage/conidium ratio) was added. Duplicate wells were assayed for each strain. The samples were incubated at 37°C with 5% CO_2 for 80 min, after which the supernatant was removed and 500 μl of 3.7% formaldehyde-PBS was added. After 15 min, the samples were washed with 1 ml of ultrapure water and incubated for 20 min with 500 μl calcofluor white (0.1 mg/ml). The samples were washed and mounted on slides with 50% glycerol. A Zeiss Observer.Z1 fluorescence microscope was used to assess the percentage of phagocytosed spores. Macrophage cells were not permeable; hence, only internalized conidia remained unstained by calcofluor white. At least 100

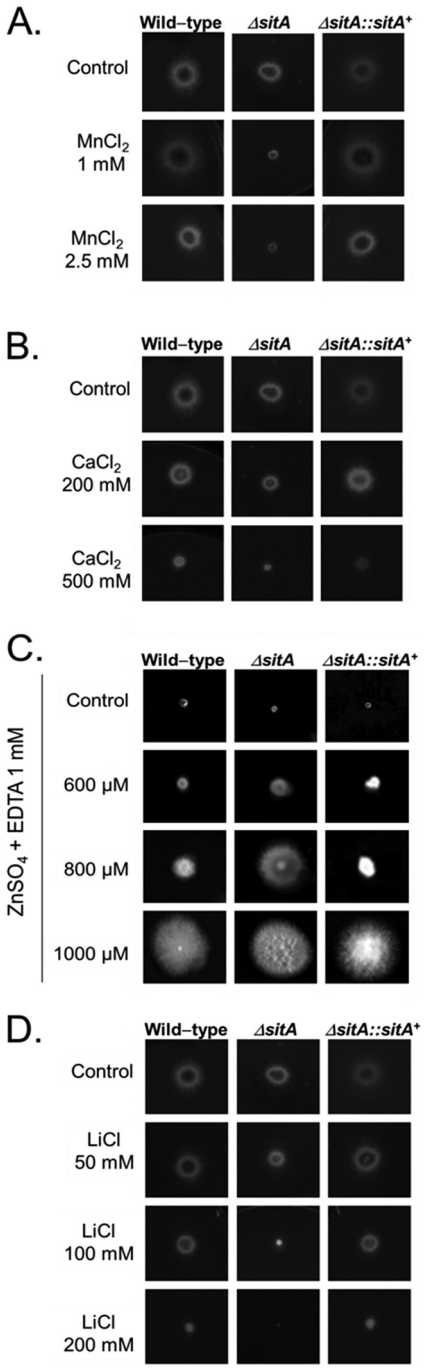

FIG 2 The *A. fumigatus* Δ*sitA* strain is more sensitive to ionic stress. The *A. fumigatus* wild-type, Δ*sitA*, and Δ*sitA*::*sitA*$^+$ strains were grown for 48 h at 37°C in MM plus different concentrations of $MnCl_2$ (A), MM plus different concentrations of $CaCl_2$ (B), MM plus different concentrations of $ZnSO_4$ plus 1 mM EDTA (C), or MM plus different concentrations of LiCl (D).

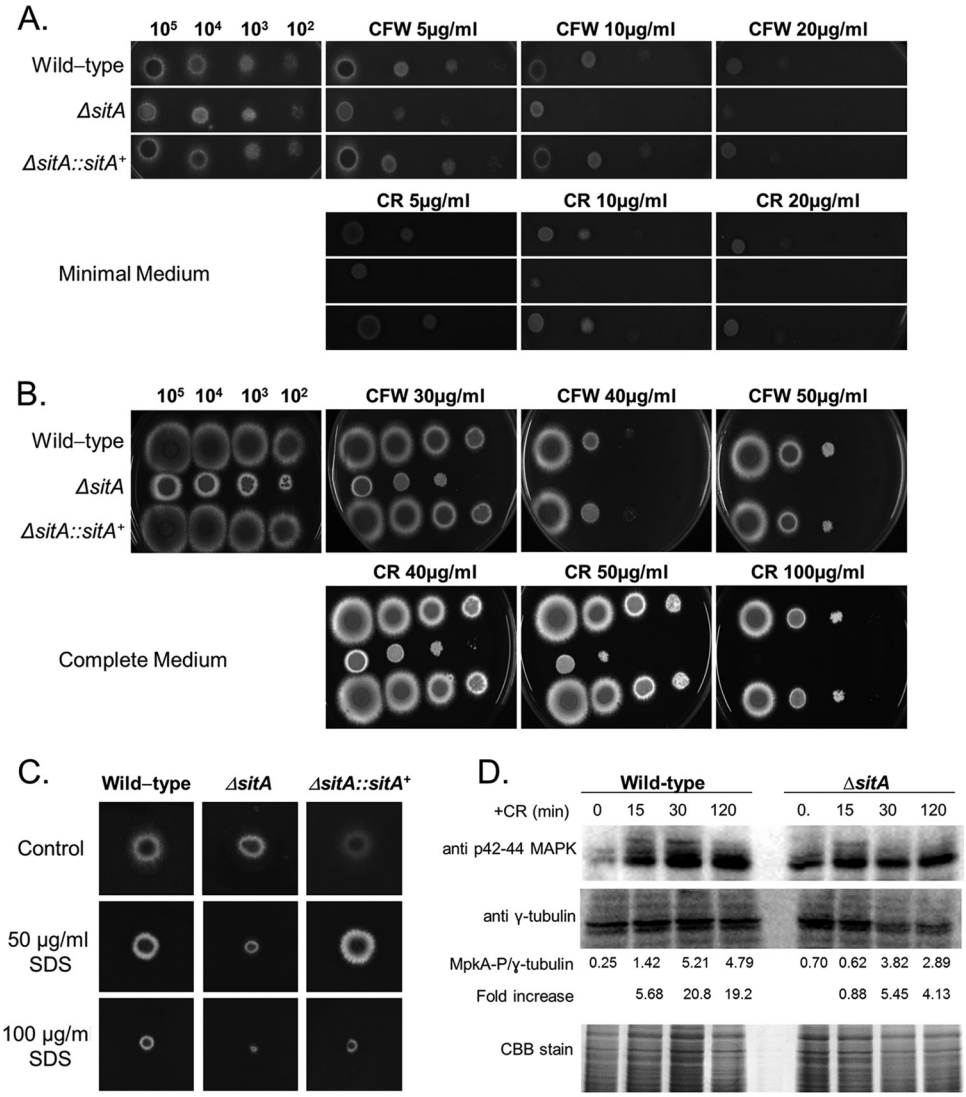

FIG 3 The *A. fumigatus* Δ*sitA* strain has impaired cell wall integrity. (A and B) The *A. fumigatus* Δ*sitA* strain is more sensitive to cell wall-damaging agents, such as CR and CFW. Conidial 10-fold dilutions (from 10^5 to 10^2) from the wild-type and Δ*sitA* and Δ*sitA*::*sitA*$^+$ mutant strains were plated on minimal (A) and complete (B) media. (C) The *A. fumigatus* Δ*sitA* strain is more sensitive to SDS. (D) Immunoblot analysis for MpkA phosphorylation in response to CFW stress. The wild type and the *sitA*-null mutants were grown for 18 h at 37°C. Then, CR (300 μg/ml) was not added (control) or was added for 15, 30, and 120 min. Anti-phospho-p44/42 MAPK antibody directed against phosphorylated MpkA was used to detect the phosphorylation of MpkA (MpkA-P). Anti-γ-tubulin antibody was used as a control for loading. A Coomassie brilliant blue (CBB)-stained gel is shown as an additional loading control. Signal intensities were quantified using Image J software by dividing the intensity of MpkA-P by that of γ-tubulin.

conidia were counted per sample, and a phagocytosis index was calculated. The experiments were repeated in triplicate.

Conidial killing by alveolar macrophages. To assess conidial killing by alveolar macrophages, the phagocytic cells were obtained as described above. In a 96-well plate, 1×10^4 macrophages were added with 200 μl of RPMI-FBS per well and incubated at 37°C with 5% CO_2 for 1 h. Afterward, 5×10^4 conidia (1:5 macrophage/conidium ratio) were added and incubated at 37°C with 5% CO_2 for 4 h. As a positive control, wells containing medium and conidia without macrophages were used. Duplicate wells were assayed for each strain with and without macrophages. After incubation, 100 μl of 3% Triton X-100 was added. After 10 min at 25°C, samples were removed from the plate and serially diluted in sterile saline. The dilutions were plated onto *A. fumigatus* complete medium (44) and incubated at 37°C for 2 days. Conidial killing was calculated by comparing CFU numbers from samples incubated with macrophages to CFU numbers from those incubated without macrophages. The experiments were repeated three times.

Determination of TNF-α levels. For cytokine determination, bone marrow-derived macrophages (BMDMs) from C57BL/6 mice were prepared as previously described (46). Briefly, bone marrow cells from femurs of adult mice were cultured for 6 days in RPMI 1640 containing 20% FBS and 30% L-929 cell conditioned medium (LCCM). Macrophages (5.0×10^5) were plated in 48-well plates for 16 h at 37°C, 5% CO_2 in RPMI 140 medium containing 10% FBS and 5% LCCM. For fungal infection, strains were cultured for 18 h to the hyphal stage at a density of 2×10^4 germlings per well, UV irradiated, and used to stimulate the macrophages. The cells were centrifuged to synchronize the infection and allowed to infect for 18 h. The supernatant was collected, and the cytokine was measured by enzyme-linked immunosorbent assay (ELISA)

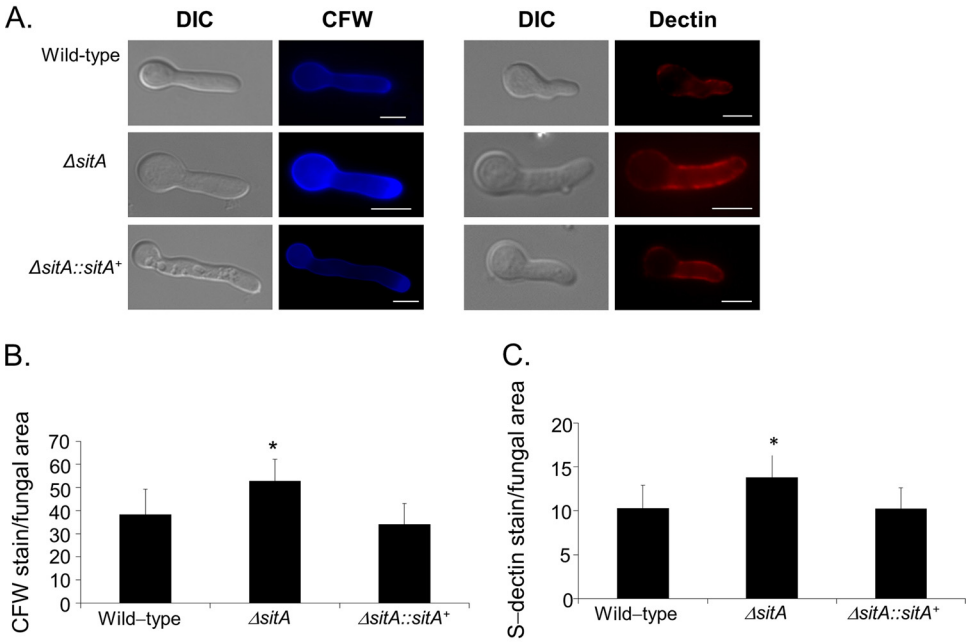

FIG 4 Detection of the β-(1,3)-glucan and chitin contents on the cell surface. Conidia were cultured in liquid medium to the hyphal stage, UV killed, and stained with soluble dectin-1 or calcofluor white (A) to detect the content of exposed chitin (B) or β-glucan (C), respectively. The intensity of staining was calculated by averaging the amount of staining to the total area of each fungal cell using ImageJ software. The experiments were performed in triplicate, and the results are displayed as arbitrary units (mean values with standard errors; * = $P < 0.05$ by *t* tests). Bars, 5 μm. DIC, differential interference contrast.

with a mouse tumor necrosis factor alpha (TNF-α) kit (R&D Quantikine ELISA) according to the manufacturer's instructions.

Inhibition of PkcA, protein extraction, and immunoblot analysis. The pharmacological inhibition of *A. fumigatus* PkcA was achieved by using chelerythrine, calphostin C, and cercosporamide. Conidia (1×10^6) of the wild-type, Δ*sitA*, and complementing strains were inoculated in 1 ml of liquid YG medium in 24-well polystyrene plates containing 10% alamarBlue (Life Technologies) as the viability indicator, according to the method of Yamaguchi et al. (47). The cells were grown for 48 h at 37°C, and growth was assessed at 24-h intervals. To assess the phosphorylation status of MpkA, fresh harvested conidia (1×10^7) of the wild-type and Δ*sitA* strains were inoculated in 50 ml liquid YG medium at 37°C for 16 h (180 rpm). After incubation, 1 μg/ml of calphostin C was added to the cultures and incubated for an additional 30, 60, and 120 min. The control was left untreated. Mycelia were ground in liquid nitrogen with a mortar and pestle. For protein extraction, 0.5 ml lysis buffer as described previously (19) containing 10% (vol/vol) glycerol, 50 mM Tris-HCl, pH 7.5, 1% (vol/vol) Triton X-100, 150 mM NaCl, 0.1% (wt/vol) SDS, 5 mM EDTA, 50 mM sodium fluoride, 5 mM sodium pyrophosphate, 50 mM β-glycerophosphate, 5 mM sodium orthovanadate, 1 mM phenylmethylsulfonyl fluoride (PMSF), and 1× Complete Mini protease inhibitor (Roche Applied Science) was added to the ground mycelium. Extracts were centrifuged at 20,000 × *g* for 40 min at 4°C. The supernatants were collected, and the protein concentrations were determined using the Bradford method (48) (Bio-Rad). Fifty micrograms of protein from each sample was resolved in 12% (wt/vol) SDS-PAGE and transferred to polyvinylidene difluoride (PVDF) membranes (Merck Millipore). The phosphorylated fraction of the MAP kinase, MpkA, was examined using anti-phospho-p44/42 MAPK antibody (9101; Cell Signaling Technologies) following the manufacturer's instructions using a 1:1,000 dilution in TBST buffer (137 mM NaCl, 20 mM Tris, 0.1% Tween 20). The primary antibody was detected using a primary goat γ-tubulin antibody and a secondary anti-goat peroxidase (HRP)-conjugated antibody (Santa Cruz Biotechnology) raised in rabbit (Sigma). Mouse anti-γ-tubulin monoclonal antibody (yN-20; Santa Cruz Biotechnology) was used as a loading control in the experiment. It was used in a 1:2,500 dilution in TBST containing 3% skim milk. Anti-γ-tubulin antibody was detected using a monkey peroxidase (HRP)-conjugated second antibody (Santa Cruz Biotechnology). Chemiluminescent detection was achieved using an ECL Prime Western blot detection kit (GE Healthcare). Images were generated by exposing the membranes to the ChemiDoc XRS gel imaging system (Bio-Rad). The images generated were subjected to densitometric analysis using ImageJ software (http://rsbweb.nih.gov/ij/index.html). The MapkA phosphorylated signal was normalized with γ-tubulin, and the values of decreased phosphorylation upon calphostin C exposure in comparison to the untreated controls are given as percentages. Detection of MpkA phosphorylation in response to Congo red (CR) stress was performed by growing the wild-type and the Δ*sitA* mutant strains for 18 h at 37°C. Then, CR (300 μg/ml) was added or not (control) for 15, 30, and 120 min.

Detection of SakA phosphorylation by Western blotting was performed as described previously (49) with slight modifications. Briefly, *A. fumigatus* conidia were inoculated into liquid YPD medium (1% yeast extract, 1% polypeptone, and 1% glucose) and cultured for 16 h prior to addition of 1/2 volume 3 M sorbitol (final concentration, 1 M). Mycelia were harvested, frozen in liquid nitrogen, and crushed in protein extraction buffer containing protease inhibitors. The suspension was centrifuged, and the supernatant was boiled with an appropriate sample buffer. Proteins were separated with a NuPAGE system (Invitrogen) and blotted using an iBlot gel transfer system (Invitrogen). To detect SakA and phosphorylated SakA proteins, a rabbit polyclonal IgG antibody against Hog1 y-215 (Santa Cruz Biotechnology, Santa Cruz, CA, USA) and a rabbit polyclonal IgG antibody against dually phosphorylated p38 MAPK (Cell Signaling Technology, Beverly, MA, USA) were used, respectively. To detect these signals on blotted membranes, the ECL Prime Western blotting detection system (GE Healthcare, Little Chalfont, United Kingdom) and LAS1000 (FujiFilm, Tokyo, Japan) were used.

RESULTS

Identification of the protein phosphatase SitA homologue in *A. fumigatus*. A BLASTp search of the *A. fumigatus* genome revealed

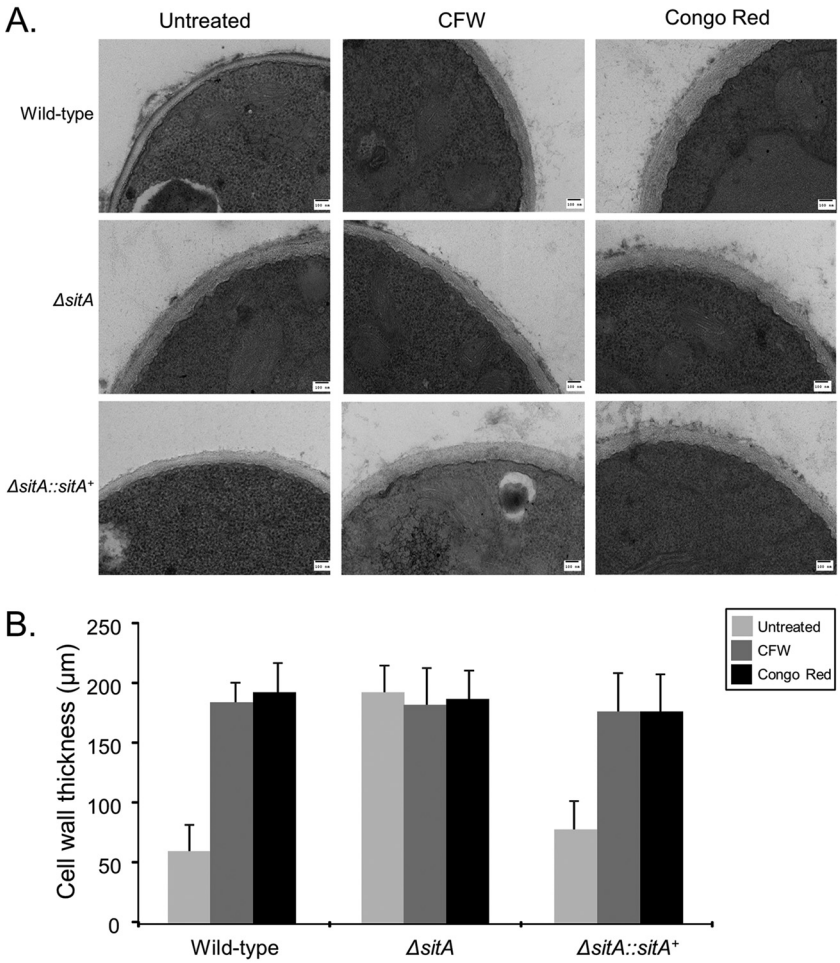

FIG 5 TEM for *A. fumigatus* wild-type and Δ*sitA* and Δ*sitA*::*sitA*$^+$ mutant strains. Germlings were grown in the absence or presence of CFW or Congo red. (A) TEM analysis (bars, 100 nm). (B) Cell wall thicknesses of 50 sections of different germlings were measured (see Table S2 in the supplemental material). The results are expressed as averages and standard deviations.

a single putative orthologue of the *S. cerevisiae* Sit4 (ScSit4), Afu6g11470 (here referred to as *sitA*). The *sitA* gene model is supported by RNA-seq data (available at http://www.aspgd.org), and three introns are predicted to be located at bp 155 to 211, 603 to 656, and 989 to 1036. The hypothetical protein encoded by *sitA* was predicted to be 388 amino acids in length and possessed a mass of 43.5 kDa. The identity between the full-length *A. fumigatus* SitA and ScSit4 proteins was high (1e−99; 72.9% identity; 84.7% similarity). A comparison of protein structures and organizations between ScSit4 and SitA was performed using the SMART interface (http://smart.embl-heidelberg.de/). The organization of the protein phosphatase 2A catalytic domains was conserved in both proteins (data not shown). Phylogenetic analyses identified numerous SitA homologues within prominent filamentous fungi (protein identity greater than 70%), including several aspergilli, plant pathogens, and saprophytic fungi (Fig. 1). However, the phylogenetic analyses clearly demonstrated two different branches from yeast and molds (Fig. 1).

The *A. fumigatus* Δ*sitA* strain has impaired cell wall integrity. To gain better insight into the function of SitA in *A. fumigatus*, the *sitA* gene was deleted (see Fig. S1 in the supplemental material) and the phenotypes of the deletion strain were compared to those of the wild-type strain. The individual gene deletion was also complemented with the corresponding wild-type gene, aiming to confirm the occurrence of possible secondary mutations during the construction of the deletion strain. Phenotypes related to *S. cerevisiae* Δ*sit4* (26, 28, 29, 50) and which could be affected by the absence of SitA, such as sensitivity to rapamycin, high osmotic stress, cell wall-damaging agents, metals, and differential growth on poor nutritional conditions, were investigated.

The Δ*sitA* strain demonstrated radial growth on both minimal and complete media comparable to that of the parental and complemented strains, except for growth at 24 h in complete medium (see Fig. S2 in the supplemental material), suggesting SitA was not important for growth under poor nutrient conditions. The Δ*sitA* strain was more sensitive to several metals and ions, such as $MnCl_2$, $CaCl_2$, and LiCl (Fig. 2A, B, and D); however, interestingly, it was more resistant to $ZnSO_4$ plus 1 mM EDTA (aiming to chelate all the preexisting metals in the medium) (Fig. 2C). The Δ*sitA* strain was as sensitive to rapamycin as the wild-type and complementing strains (see Fig. S3 in the supplemental material) and was more sensitive to cell wall-damaging agents, such as CR, CFW, and SDS (Fig. 3A to C).

To determine if SitA was involved in the Mpk1 pathway in *A.*

fumigatus, the amount and phosphorylation state of the Mpk1p homologue, MpkA, were determined in the presence and absence of CR stress. The phosphorylation level of the MpkA protein was determined using the anti-p44/42 MAPK antibodies directed against phosphorylated MpkA (Fig. 3D). In the wild-type strain, MpkA phosphorylation levels increased 5.68-, 20.8-, and 19.2-fold posttransfer to 300 μg/ml CR for 15, 30, and 120 min, respectively (Fig. 3D). The Δ*sitA* strain had about 3-fold-higher MpkA phosphorylation levels than the wild-type strain in the absence of CR (Fig. 3D). However, the Δ*sitA* mutant demonstrated levels of MpkA induction of 0.88-, 5.45-, and 4.13-fold posttransfer to 300 μg/ml CR for 15, 30, and 120 min (Fig. 3D). The MpkA phosphorylation levels in the Δ*sitA* mutant were about 4- to 5-fold lower than those in the wild-type strain (Fig. 3D).

This increased sensitivity to cell wall-damaging agents could be due to alterations in cell wall organization. Thus, fungal cell wall chitin levels were assessed via CFW staining. The intensity of CFW staining per fungal area was 20% higher in the Δ*sitA* mutant than in the wild-type strain (Fig. 4A and B). Soluble dectin-1 staining was used to identify differences in the content, or exposure, of β-(1,3)-glucans on the surface of the fungal cell wall in both the wild-type and Δ*sitA* strains. The Δ*sitA* strain was shown to have a higher level of β-glucans than the wild-type and complemented Δ*sitA*::*sitA*$^{+}$ strains. The intensity of dectin-1 staining per fungal area was 40% higher in the Δ*sitA* mutant than in the wild-type strain (Fig. 4A and C). Collectively, these results suggest that the surface of the Δ*sitA* cell had more abundant chitin and β-(1,3)-glucans than the wild-type strain. Differences in susceptibility to caspofungin (greater resistance) were observed in the Δ*sitA* strain (see Fig. S4 in the supplemental material). Additional evidence for a role of SitA in the organization of the cell wall was provided by TEM analysis (Fig. 5A). Untreated Δ*sitA* germlings grown in MM had about 3-fold-thicker cell walls than the wild-type and the complementing strains (Fig. 5B; see Table S2 in the supplemental material). Further exposure of the Δ*sitA* germlings to CFW and Congo red did not change the cell wall thickness (Fig. 5B; see Table S2 in the supplemental material). In contrast, when the wild-type and the complementing strains were exposed to CFW and CR, they had about 2.5- to 3-fold-increased cell wall thickness (Fig. 5B; see Table S2 in the supplemental material). Taken together, these results strongly indicate that SitA is important for the *A. fumigatus* cell wall integrity pathway.

The *A. fumigatus* Δ*sitA* strain has reduced adhesion properties. The altered composition of the cell wall could also alter the adhesion of conidia and/or mycelia to surfaces or other fungal cells. The Δ*sitA* conidia showed a drastic alteration in hydrophobicity and reduction in the hydrophobin RodA content (Fig. 6A and B). The ability to form biofilms on solid surfaces was assessed. Biofilm formation evaluated by CV and biomass accumulation was decreased about 40 to 60% and 20%, respectively (Fig. 6C and D). SEM of the mycelia revealed that SitA influenced the cell surface and the extracellular matrix during biofilm formation (Fig. 7). The surface of the Δ*sitA* strain appeared smooth, which was in stark contrast to that of the wild-type strain (Fig. 7). Collectively, this demonstrates that SitA influences the conidial and hyphal surfaces, impacting upon hydrophobicity, adhesion, and biofilm formation.

We also investigated the total cell surface proteins in the Δ*sitA* strain compared to the wild type by extraction of cell surface proteins using 0.5 M NaCl (41). The proteins extracted from the

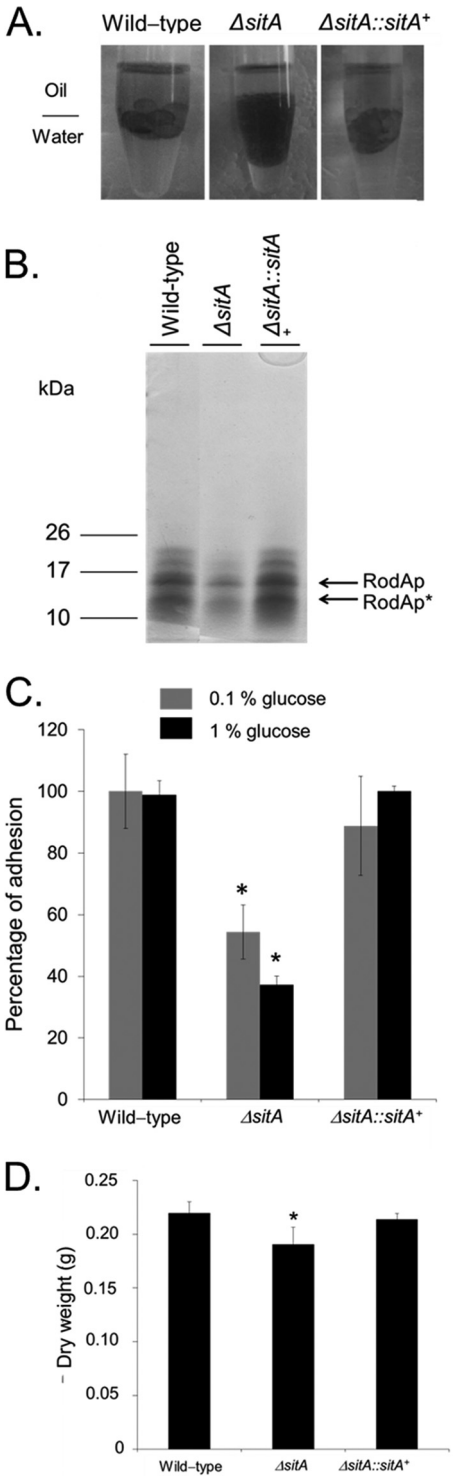

FIG 6 The *A. fumigatus* Δ*sitA* strain has reduced adhesion properties. (A) Fungal adhesion and biofilm formation are influenced by *sitA*. Shown are wild-type and Δ*sitA* conidia in a 1:1 water-oil (tributyrin) interface. (B) Polyacrylamide gel showing the hydrophobin concentrations of wild-type, Δ*sitA*, and Δ*sitA*::*sitA*$^{+}$ conidia. RodAp corresponds to the native RodA and RodAp* to partially degraded or processed RodA. (C) Adhesion, measured by CV assay, is reduced in the Δ*sitA* mutant in both 0.1% and 1% glucose (*, $P < 0.01$ compared to the wild-type strain). (D) Biofilm formation is reduced in the Δ*sitA* mutant. The error bars indicate standard deviations.

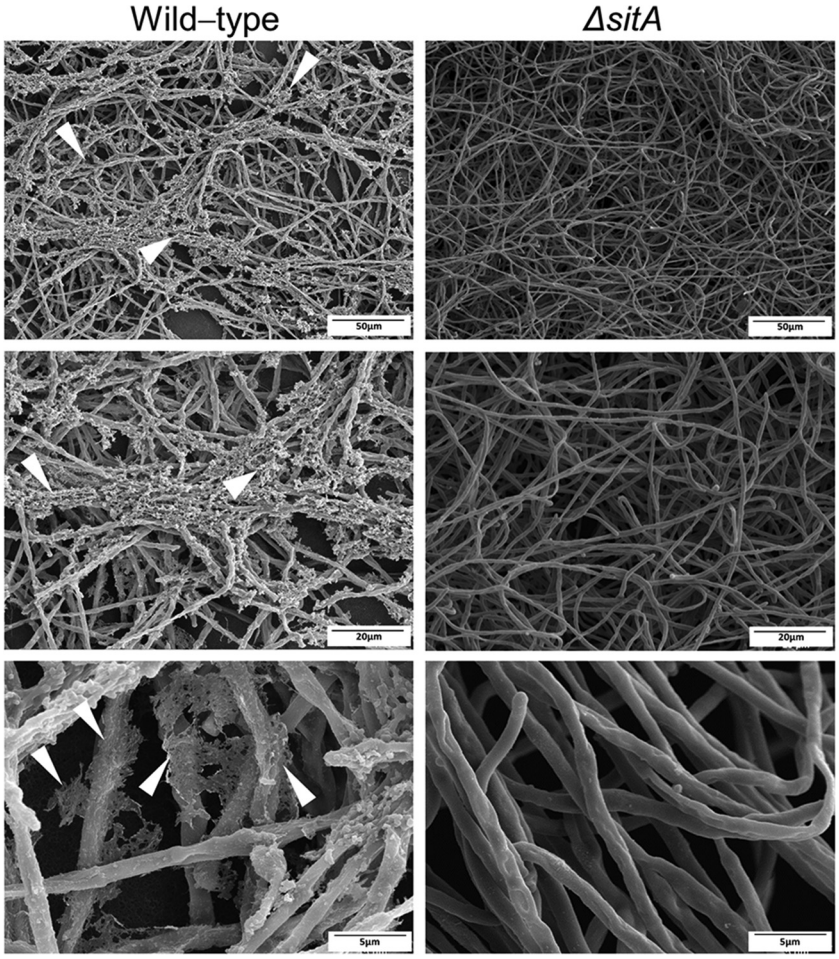

FIG 7 Scanning electron microscopy for the wild-type and Δ*sitA* mutant strains. Magnification, ×1,000. The arrowheads indicate the extracellular matrix.

conidial surface from both strains were analyzed by LC–MS-MS (see Table S3 in the supplemental material). We were able to identify in both strains 213 conidial surface proteins (see Table S3 in the supplemental material), but only 52 of them are differentially expressed in the two strains (Table 1). Twenty-two of these differentially expressed proteins are either absent in the Δ*sitA* strain (11 proteins) but present in the wild type or present in the Δ*sitA* strain (also 11 proteins) but absent in the wild type (Table 1). Fifty percent of the proteins are enzymes, and most of them are involved in remodeling of the cell wall, such as NagA (*N*-acetylhexosaminosidase) and Gel1 (1,3-beta-glucanosyltransferase; *gelA*) (Table 1). Forty percent are hypothetical proteins, and 10% are adhesin-like proteins (Table 1). Fourteen of these 52 proteins were more highly expressed in the Δ*sitA* mutant strain (Table 1). These proteins comprise 7 enzymes, 2 belonging to the translation machinery, and 2 allergens (Aspf13 and Aspf34) (Table 1). Sixteen proteins were more highly expressed in the wild-type strain: 8 enzymes, 1 protein related to the translation machinery, 1 toxin, 5 hypothetical proteins, and 1 allergen (Aspf1) (Table 1). These results imply that SitA is important for the proper conidial surface protein distribution that is revealed by NaCl extraction.

The Δ*sitA* mutant is more sensitive to protein kinase C inhibitors. The *S. cerevisiae* Sit4p phosphatase is required for the correct downregulation of both basal and induced activities of PKC1 (26). Calphostin C, chelerythrine, and cercosporamide have been used as protein kinase C inhibitors in mammals and in fungi (51–56). We hypothesize if Δ*sitA* modulated the protein kinase C activity, the susceptibility status of Δ*sitA* to these inhibitors would be altered. Growth of the Δ*sitA* strain was dramatically inhibited by calphostin C, cercosporamide, and chelerythrine (Fig. 8A to C). This was further confirmed by reduced MpkA phosphorylation in the Δ*sitA* mutant compared to the wild-type strain when both strains were exposed to calphostin C (Fig. 8D). These results strongly suggest that the Δ*sitA* strain has reduced protein kinase C activity and that it probably modulates the expression of protein kinase C.

SitA is important for *A. fumigatus* virulence in a low-dose murine infection. The importance of SitA to *A. fumigatus* pathogenicity was evaluated in a neutropenic murine model of invasive pulmonary aspergillosis (Fig. 9A). Infection with the wild-type strain resulted in 100% mortality 12 days postinfection, while infection with the Δ*sitA* strain resulted in a significantly reduced mortality rate, approximately 15%, 15 days postinfection (Fig. 9A) ($P < 0.0003$ and $P < 0.0007$ for comparison between the wild type and the deletion mutant; log-rank [Mantel-Cox] and Gehan-Breslow-Wilcoxon tests, respectively). Virulence was restored in an independent strain that resulted from a single ectopic reintegration of the wild-type *sitA* locus, and there was no statistical

TABLE 1 Conidial surface proteins identified in the wild-type and Δ*sitA* mutant strains

A. fumigatus protein	Function	Mass (kDa)	Length (aa[a])	Ratio (Δ*sitA*/WT)[b]	% coverage[c]	
					Mutant	WT
Conidial surface proteins absent in the Δ*sitA* mutant strain						
Afu1g17410	Beta-glucosidase	84	782	Only in WT	NI	2
Afu3g14030	Alkaline phosphatase, *phoB* regulated	72	653	Only in WT	NI	17
Afu2g00690	Glucan 1,4-alpha-glucosidase activity; role in polysaccharide metabolic process and Golgi apparatus, endoplasmic reticulum, and prospore membrane localization	67	631	Only in WT	NI	6
Afu2g17530	Laccase involved in conidial pigment biosynthesis	65	587	Only in WT	NI	15
Afu7g05140	Putative class III family 18 chitinase	46	448	Only in WT	NI	16
Afu3g00270	Cell wall glucanase; predicted glycophosphatidylinositol (GPI) anchor; secreted protein	44	450	Only in WT	NI	5
Afu2g05240	Orthologues have extracellular region localization	42	400	Only in WT	NI	11
Afu2g00680	Open reading frame (ORF), uncharacterized; has domain(s) with predicted catalytic activity	40	375	Only in WT	NI	8
Afu7g05650	ORF, uncharacterized; orthologue of *A. fumigatus* A1163 (AFUB_091230)	23	225	Only in WT	NI	8
Afu5g01420	ORF, uncharacterized; orthologue(s) have extracellular region localization	22	205	Only in WT	NI	30
Afu2g13600	Pyruvate dehydrogenase (acetyl-transferring) kinase activity; role in carbon utilization, peptidyl-serine phosphorylation, and mitochondrion localization	20	187	Only in WT	NI	8
Conidial surface proteins absent in the WT strain						
Afu8g05020	NagA, secreted *N*-acetylhexosaminidase; highly expressed in biofilm	67	600	Only in Δ*sitA*	8	NI
Afu2g02100	Dihydrolipoamide dehydrogenase; reacts with rabbit immunosera exposed to *A. fumigatus* conidia	54	513	Only in Δ*sitA*	27	NI
Afu2g01170	Gel1, 1,3-beta-glucanosyltransferase with a role in elongation of 1,3-beta-glucan chains; GPI-anchored protein; constitutively expressed during hyphal growth; hypoxia-induced protein	48	452	Only in Δ*sitA*	6	NI
Afu7g05740	NAD-dependent malate dehydrogenase; protein abundant in conidia; immunoreactive; reacts with rabbit immunosera exposed to *A. fumigatus* conidia; induced by L-tyrosine; transcript downregulated in response to hypoxia	35	340	Only in Δ*sitA*	17	NI
Afu6g10930	ORF, uncharacterized; protein of unknown function	30	290	Only in Δ*sitA*	8	NI
Afu6g14370	AraC-like ligand binding domain protein	23	213	Only in Δ*sitA*	9	NI
Afu3g00880	Putative adhesin protein; MedA-regulated transcript; transcript repressed by exposure to human airway epithelial cells	21	219	Only in Δ*sitA*	13	NI
Afu3g09390	Laminin-binding protein with extracellular thaumatin domain; predicted adhesin-like protein; expression induced in biofilm; repressed by exposure to artemisinin	18	177	Only in Δ*sitA*	14	NI
Afu1g01980	ORF, uncharacterized; orthologue(s) have role in hyphal growth, response to cold, response to heat, response to oxidative stress, response to salt stress, sporocarp development involved in sexual reproduction	18	179	Only in Δ*sitA*	6	NI
Afu5g01990	ORF, uncharacterized; BYS1 domain protein	16	156	Only in Δ*sitA*	12	NI
Afu4g09320	DppIV, extracellular dipeptidyl-peptidase; predicted signal sequence for secretion; induced by growth on BSA as a sole nitrogen source; expression dependent on PrtT	85	765	30.5	18	NI
Conidial surface proteins more highly expressed in the Δ*sitA* mutant strain						
Afu5g10490	Amidase; secreted protein; fibrinogen binding	65	611	18.8	5	3
Afu5g03540	Orthologues have flavin-linked sulfhydryl oxidase activity and roles in oxidation-reduction process and extracellular region localization	42	386	11.7	12	14
Afu4g13750	Mep20, penicillolysin/deuterolysin metalloprotease; predicted signal sequence for secretion	39	370	9.6	5	5
Afu1g06390	Tef1, translation elongation factor EF-1 alpha subunit; protein abundant in conidia; protein induced by heat shock	53	494	4.9	14	3
Afu3g08290	Aspartyl aminopeptidase; immunoreactive; secreted protein; induced by growth on BSA as a sole nitrogen source	54	504	3.9	6	5
Afu8g00710	ORF, uncharacterized; has domain(s) with predicted role in defense response, negative regulation of growth	10	101	3.2	34	48
Afu2g09030	DppV, secreted dipeptidyl-peptidase; induced by growth on BSA as a sole nitrogen source; immunoreactive protein	79	721	2.9	24	12
Afu7g07010	Adh1, alcohol dehydrogenase; predicted gene pair with AFUA_5G06240 (*alcC*); induced by L-tyrosine; transcript upregulated in conidia exposed to neutrophils	37	353	2.0	5	4

(Continued on following page)

TABLE 1 (Continued)

A. fumigatus protein	Function	Mass (kDa)	Length (aa[a])	Ratio (Δ*sitA*/WT)[b]	% coverage[c]	
					Mutant	WT
Afu5g09240	Sod1, Cu/Zn superoxide dismutase; recognized by sera from aspergillosis patients; highly expressed in conidia; transcript induced by copper starvation, menadione, gliotoxin, and growth at high temp; protein induced by hydrogen peroxide	15	154	2.0	28	30
Afu3g02270	Cat1, mycelial catalase; induced in hyphae exposed to neutrophils; protein induced in amphotericin B and H_2O_2; *stuA*-dependent upregulation in developmentally competent hyphae; hypoxia repressed; SrbA regulated; repressed by gliotoxin exposure	79	728	2.0	22	21
Afu5g01120	ORF, uncharacterized; orthologue of *Aspergillus nidulans* FGSC A4 (AN8927), *Aspergillus oryzae* RIB40 (AO090003001298), *Aspergillus flavus* NRRL 3357 (AFL2T_01773), and *Neosartorya fischeri* NRRL 181 (NFIA_041050)	36	354	1.8	4	9
Afu2g12630	Aspf13, allergen Asp f 13; putative alkaline serine protease; higher expression in biofilm than in planktonic cells; transcript induced by growth on hydrogen peroxide	15	152	1.8	43	44
Afu3g03060	Aspf34, allergen Asp f 34; putative PhiA family cell wall protein; induced by calcium; repressed by exposure to artemisinin	19	185	1.8	9	9
Afu1g12070	ORF, uncharacterized; orthologues have glycine dehydrogenase (decarboxylating) activity, roles in glycine catabolic process, one-carbon metabolic process, protein lipoylation, and mitochondrion localization	18	175	1.6	9	9
Afu3g15090	Adenosine deaminase family protein; secreted protein; predicted secretory signal sequence; orthologue of *A. nidulans* AN2494	66	587	1.3	16	15
Conidial surface proteins more highly expressed in the WT						
Afu1g15730	40S ribosomal protein S22	14	130	0.9	11	11
Afu1g14450	ExgO, exo-beta-1,3-glucanase; secreted protein; predicted secretory signal sequence; orthologue of *A. nidulans* AN0779	10	947	0.8	10	13
Afu3g07030	Gta1, glutaminase A; secreted protein; predicted secretory signal sequence	76	691	0.8	16	20
Afu3g00590	AspHS, Asp-hemolysin; hemolytic toxin; highly secreted; enriched in conidia; expression increases *in vivo*; binds lysophosphatidylcholine	15	139	0.7	20	25
Afu1g05770	Exg12, secreted beta-glucosidase; predicted secretory signal sequence; fibrinogen binding	94	873	0.6	10	20
Afu1g10970	Alpha-1,2-mannosidase family protein	92	839	0.6	2	19
Afu6g14470	Orthologue of *A. nidulans* FGSC A4 (AN5353), *Aspergillus niger* CBS 513.88 (An02g05680), *A. oryzae* RIB40 (AO090103000108), *Aspergillus wentii* (Aspwe1_0131073), and *Aspergillus sydowii* (Aspsy1_0050268)	26	234	0.5	10	18
Afu2g00967	Orthologue of *A. nidulans* FGSC A4 (AN7635/binA and AN11904), *A. fumigatus* Af293 (Afu3g02216 and Afu7g00610), and *A. niger* CBS 513.88 (An10g00560)	21	196	0.5	7	8
Afu6g03210	ConJ, protein of unknown function; conidium-enriched protein; orthologue of *Neurospora crassa*	87	83	0.4	35	26
Afu8g00630	Uncharacterized; Orthologues have extracellular region localization	37	347	0.3	27	41
Afu4g09280	ORF, uncharacterized; orthologue of *A. niger* CBS 513.88 (An02g00330), *Neosartorya fischeri* NRRL 181 (NFIA_106720), *A. niger* ATCC 1015 (36613-mRNA), and *Aspergillus carbonarius* ITEM 5010 (Acar5010_203109)	18	167	0.2	28	54
Afu4g11800	Alp1, secreted alkaline serine protease; cleaves human complement components C3, C4, and C5; predicted signal sequence for secretion; fibrinogen binding	42	403	0.2	12	22
Afu6g12070	FmqD, flavoprotein amide oxidase (FAD); has FAD activity; member of the fumiquinazoline-biosynthetic cluster; may contain an N-terminal signal sequence and multiple N-glycosylation sites; transcript downregulated in response to voriconazole	54	497	0.2	5	14
Afu1g14560	MsdS, 1,2-alpha-mannosidase; secreted protein; fibrinogen binding	53	493	0.2	2	7
Afu7g06140	Exg13, secreted 1,4-beta-D-glucan glucanhydrolase	78	739	0.1	2	7
Afu5g02330	Aspf1, Aspf1 antigen/allergen; RNase mitogillin family of cytotoxins; similar to restrictocin; inhibits protein synthesis in mammalian cells; 18-kDa IgE-binding protein; expression increases *in vivo*; biofilm-induced vs planktonic cells	19	176	0.05	7	17

[a] aa, amino acids.
[b] The values are related to the spectral counts of three repetitions for each strain. WT, wild-type strain.
[c] NI, not identified.

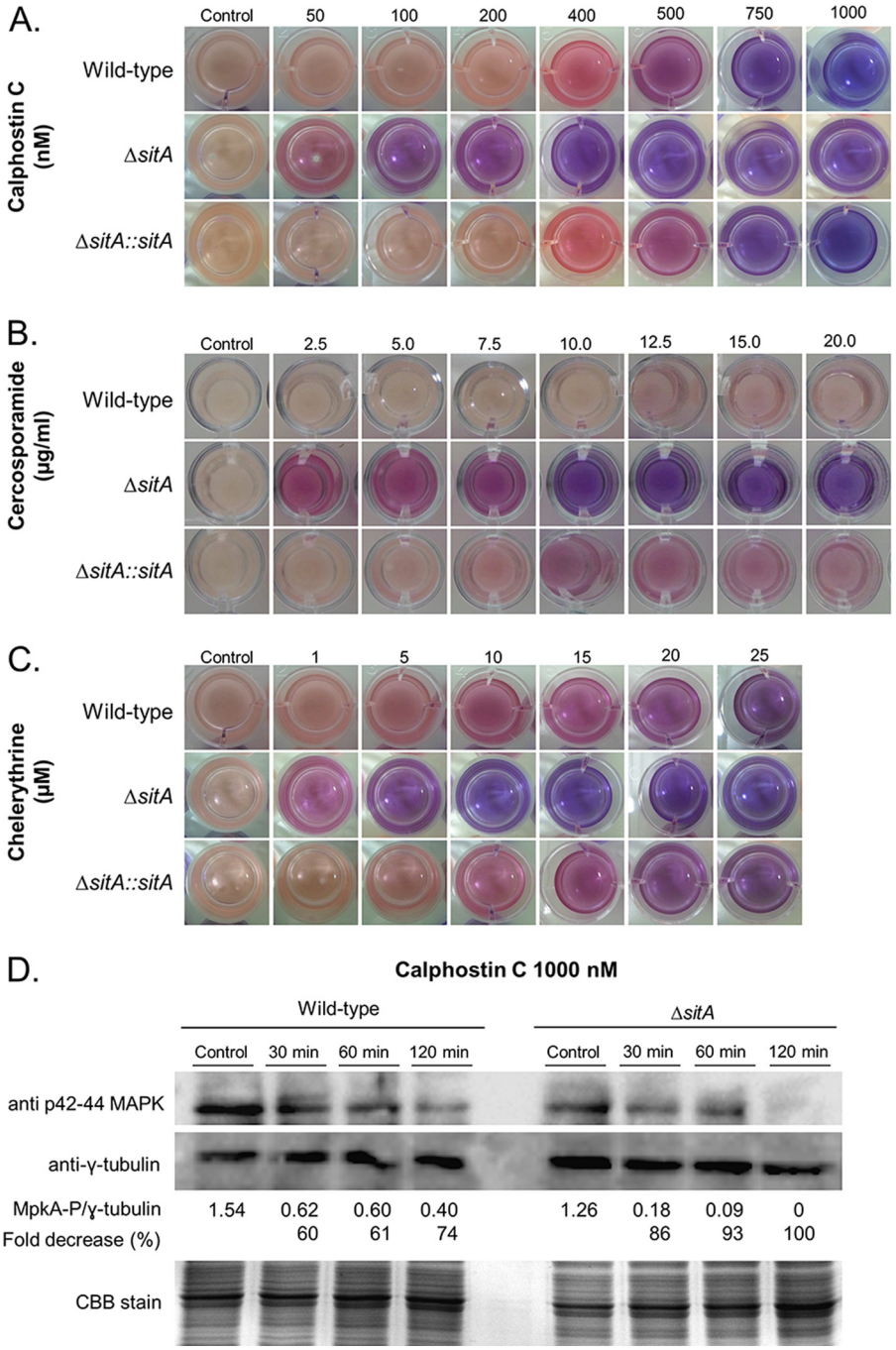

FIG 8 The Δ*sitA* strain has reduced protein kinase activity. (A to C) Viability of the germlings of the wild-type, Δ*sitA*, and Δ*sitA*::*sitA*$^+$ strains grown in the absence or presence of calphostin C, cercosporamide, and chelerythrine as shown by the viability indicator alamarBlue. The germlings are less viable when the indicator shows intensely blue colonies, indicating decreased mitochondrial activity. Pink and red indicate viability. (D) Western blot for MpkA phosphorylation. The wild-type and Δ*sitA* strains were grown for 16 h at 37°C, and then mycelia were transferred to fresh medium with calphostin C for 30, 60, and 120 min. Anti-phospho-p44/42 MAPK antibody directed against phosphorylated MpkA was used to detect the phosphorylation of MpkA. Anti-γ-tubulin antibody was used as a control for loading. A CBB-stained gel is shown as an additional loading control. The signal intensities were quantified using Image J software by dividing the intensity of MpkA-P by that of γ-tubulin.

difference between the wild-type and the complemented Δ*sitA*::*sitA*$^+$ strains (Fig. 9A) ($P > 0.3$ and $P > 0.4$ for comparison between the wild-type and the complemented strain; log rank, Mantel-Cox, and Gehan-Breslow-Wilcoxon tests, respectively), directly linking the attenuation of Δ*sitA* virulence to the SitA function.

Histopathological examination revealed that at 72 h postinfection, the lungs of mice infected with the wild-type strain contained multiple foci of invasive hyphal growth, which penetrated the pulmonary epithelium in major airways, while pockets of branched invading hyphae originated from the alveoli (Fig. 9B). In contrast, Δ*sitA* infections revealed inflammatory infiltrates in bronchioles,

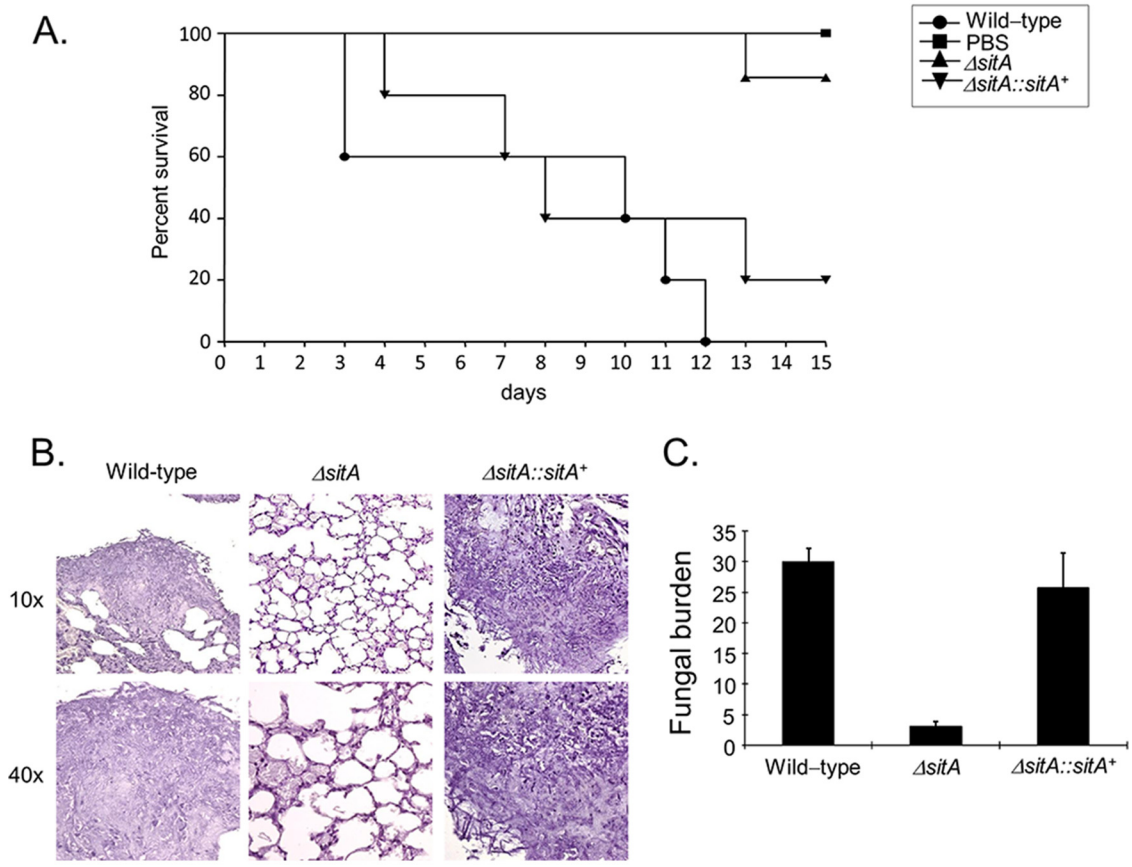

FIG 9 The *A. fumigatus* Δ*sitA* strain contributes to virulence in neutropenic mice. (A) Comparative analysis of wild-type and mutant strains in a neutropenic murine model of pulmonary aspergillosis. Mice in groups of 10 per strain were infected intranasally with a 20-μl suspension of conidiospores at a dose of 10^5 conidiospores. (B) Histological analysis of infection in the murine lung was performed 72 h after infection. (C) Fungal burden results, determined by qPCR at 72 h postinfection, were expressed based on the 18S rRNA gene of *A. fumigatus* divided by the results of an intronic region of the mouse GAPDH gene.

with some containing poorly germinated or ungerminated conidia (Fig. 9B). The fungal burden was measured by quantitative PCR (qPCR), showing that the Δ*sitA* strain did not grow within the lungs as well as the wild-type and the complemented Δ*sitA*::*sitA*$^+$ strains (Fig. 9C). Taken together, the data strongly indicate that SitA plays an important role in *A. fumigatus* virulence.

The impaired Δ*sitA* CWI, together with the dramatic attenuation in virulence, could contribute to an altered immune response. AMs play an essential role in clearing *A. fumigatus* conidia from the lung (57). Approximately 15% of *A. fumigatus* wild-type and Δ*sitA*::*sitA*$^+$ conidia were internalized after 80 min of incubation with AMs (Fig. 10A). In contrast, about 40% of Δ*sitA* conidia were internalized after the same period (Fig. 10A). After 4 h of incubation, no differences in the *in vitro* killing of resting conidia for the *A. fumigatus* wild-type, Δ*sitA*, and Δ*sitA*::*sitA*$^+$ strains was observed (data not shown). These data suggest that the Δ*sitA* strain is more sensitive to phagocytosis, while there are no differences in AM killing for all three strains. Subsequently, levels of the cytokine TNF-α released from BMDMs after coincubation with *A. fumigatus* hyphae were investigated. TNF-α is an important inflammatory mediator secreted by macrophages when exposed to *A. fumigatus* (58, 59). BMDMs cocultured with the Δ*sitA* strain show higher TNF-α production than the wild-type or the complemented strain (about 2.4-fold) (Fig. 10B). These results suggest that the effect caused by SitA on the CWI is important for macrophage recognition and inducing inflammatory responses.

DISCUSSION

A. fumigatus is a cosmopolitan fungus and is able to live and survive in different environments. This ability requires it to possess great metabolic versatility and the capability to adapt to these diverse ecological niches through the precise regulation of a complex network of signaling cascades and their downstream effects. *A. fumigatus* efficiently utilizes the human body as a niche, causing several clinical forms of disease, depending on the status of the human immune system. How *A. fumigatus* is able to overcome host defenses and establish infection is dependent on the coordination of these signal transduction pathways. An enhanced understanding of these mechanisms of adaptation may have impacts on the establishment of strategies to control the disease. Recently, as an initial step to comprehend the signaling pathways regulating the program of adaptation, we methodically investigated all 32 *A. fumigatus* phosphatase-encoding genes and constructed a collection of 24 null mutants for these genes (reference 31 and unpublished results). Here, we focused on a single phosphatase, SitA, in greater detail and assigned it a role in cell signaling and virulence.

The *A. fumigatus* gene *sitA* codes for a Ser/Thr protein phos-

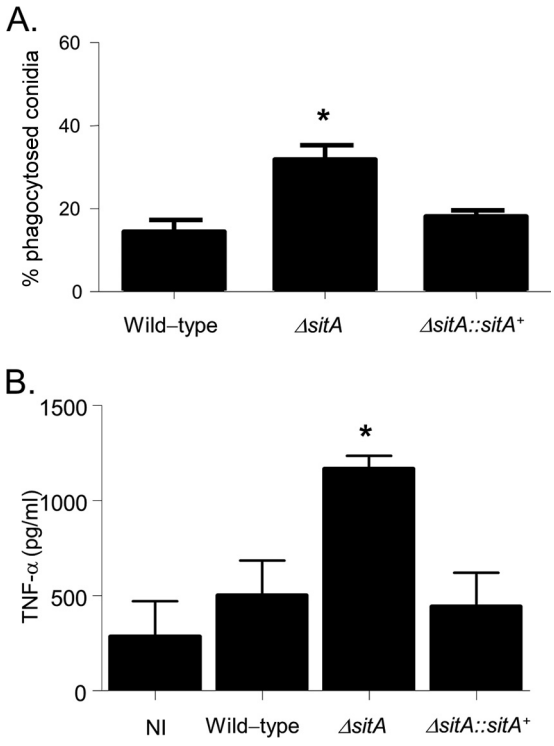

FIG 10 Macrophage recognition and TNF-α secretion from BMDMs. (A) There is increased uptake of Δ*sitA* conidia by AM phagocytes. Shown are the percentages of conidia taken up by AMs. The number of conidia phagocytosed is increased for the Δ*sitA* strain. The data are shown as averages and standard deviations. *, $P < 0.01$ compared to the wild-type and the complemented strains. (B) Δ*sitA* hyphae trigger significantly increased release of TNF-α from BMDMs compared to the wild-type and the reconstituted strains. BMDMs from C57BL/6 mice were infected with *A. fumigatus* hyphae for 18 h, and the supernatant of the cells was collected to measure the TNF-α levels by ELISA. The data are shown as averages and standard deviations. *, $P \leq 0.005$ compared to the wild-type and the complemented strains. NI, noninfected.

phatase member of the PPP phosphatase family, which is closely related to the PP2A family. In *S. cerevisiae*, Sit4p plays a critical role in cell growth and proliferation and is involved in several biological processes, such as the TOR pathway-mediated response to nutrients (60–63), the regulation of monovalent ion homeostasis and intracellular pH (64), and cell cycle regulation (28, 65), and is required for proper telomere function (66), the initiation of translation (67), and the CWI pathway (26). We have observed that the *A. fumigatus sitA*-null mutant has neither growth defects nor developmental problems. *S. cerevisiae* Sit4p is phosphorylated by TOR, negatively regulating Sit4p through the association of Sit4p with Tap42p. The main signals for Sit4p activation are treatment with rapamycin and nitrogen starvation (30). When Sit4p is activated, downstream effectors of TOR are dephosphorylated in a Sit4p-dependent manner (30). The *A. fumigatus* Δ*sitA* strain was not more sensitive to rapamycin than the wild-type strain, and we also have not observed any nutritional impairment in the strain. Sit4 homologues have been characterized in only two other fungi, *Candida albicans* and *Fusarium graminearum* (61, 68). In *C. albicans*, *SIT4* homologue disruption resulted in a reduced growth rate and virulence in a mouse infection model (68). The authors observed that *C. albicans* Sit4p was involved in hyphal growth by regulating cell wall biogenesis, osmosensing, and protein translation. More recently, Sit4p was identified as a potential regulator of the early hypoxic response in *C. albicans* (69). Prior to this work, only one Sit4 homologue had been described in filamentous fungi, FgSIT4 in *F. graminearum* (61). In the plant pathogen *F. graminearum*, FgSit4 plays important roles in regulation of various cellular processes, including mycelium growth, virulence, and sexual development (61). FgSit4 affects the cell wall integrity pathway by positively regulating the phosphorylation of FgMgv1, the key MAP kinase in the CWI pathway.

The *A. fumigatus* cell wall is mainly composed of polysaccharides, such as branched β-(1,3)-glucan, to which chitin, β-(1,3)-/β-(1,4)-glucan, and galactomannan are covalently bound, and α-(1,3)-glucan, which has adhesive properties and stabilizes the cell wall (42). The conidial cell wall is covered by an outer layer of rodlets and melanin, which possess hydrophobic properties, as well as being immunologically inert (70–72). The outer layer has galactosaminogalactan, while the mycelium grows embedded in an extracellular matrix rich in polysaccharides, hydrophobins, and melanin (42). We have observed that the *A. fumigatus* Δ*sitA* conidia have reduced hydrophobin content, while the mutant is sensitive to cell wall-damaging agents and has increased MpkA phosphorylation. Moreover, *A. fumigatus* Δ*sitA* germlings have altered cell wall organization, and the hyphae have reduced adhesion, biofilm formation, and extracellular matrix production. The conidial surface protein profile of the Δ*sitA* mutant is also distinct from that of the wild type. However, quantitative analyses of cell wall components in the Δ*sitA* strain remain for future investigation. All these defects strongly suggest defects in the CWI pathway. The protein kinase C-mediated mitogen-activated protein kinase (PKC1-MAPK) pathway is essential for activation of the CWI in fungi (12, 73). The *S. cerevisiae SIT4*Δ strain has a G_1-to-S delay in the cell cycle, which is mediated by the upregulation of Pkc1 activity (26). In *S. cerevisiae*, Sit4 operates downstream of the plasma membrane sensors Mid2, Wsc1, and Wsc2 and upstream of Pkc1, affecting Pkc1 functions, such as Mpk1 activity and the CWI, actin cytoskeleton organization, and ribosomal gene transcription (26). It remains to be investigated whether, in *A. fumigatus*, SitA directly or indirectly modulates PkcA or other targets that are involved in the CWI pathway. We have observed that the Δ*sitA* mutant has reduced MpkA phosphorylation when exposed to cell wall-damaging agents and is more sensitive to protein kinase C inhibitors, suggesting the PkcA activity in the mutant is lower than in the wild-type strain. This is further emphasized by the reduced MpkA phosphorylation in this mutant in the presence of these inhibitors.

We have shown that the Δ*sitA* strain has attenuated virulence and increased recognition by macrophages. In the immunosuppressed murine model of invasive pulmonary aspergillosis, the Δ*sitA* strain is avirulent compared to the wild-type and complemented strains. TNF-α, one of the key inflammatory mediators secreted by macrophages in response to fungal hyphae, was increased in the Δ*sitA* strain compared to the wild-type and complemented strains. This proinflammatory cytokine plays an important role in the induction of the innate immune response to *A. fumigatus* (59, 66). The increased β-(1,3)-glucan, reduced hydrophobin content, and other modifications in the Δ*sitA* cell wall could contribute to an increased recognition of the fungus by the dectin receptor, favoring its increased phagocytosis by alveolar macrophages and, consequently, increased TNF-α production, since β-glucan is a potent stimulator of the TNF-α response in fungi (74–77).

In summary, we have demonstrated that SitA is an important

phosphatase for cell wall construction and is essential for virulence and macrophage recognition. How SitA affects the organization of the cell wall remains to be investigated. However, based on *S. cerevisiae* studies, it is likely that SitA modulates the PkcA activity. This improved understanding of the function of SitA in *A. fumigatus* may in turn provide an opportunity to improve our knowledge of how *A. fumigatus* regulates cell wall integrity and composition during virulence.

ACKNOWLEDGMENTS

We thank the Conselho Nacional de Desenvolvimento Científico e Tecnológico (CNPq) and the Fundação de Amparo à Pesquisa do Estado de São Paulo (FAPESP) for providing financial support.

We thank the Microscopy and Histology Facility of the Institute of Medical Sciences, University of Aberdeen, Aberdeen, Scotland, United Kingdom, for performing the SEM. We also thank the two anonymous reviewers for their comments and suggestions.

REFERENCES

1. **Dagenais TR, Keller NP.** 2009. Pathogenesis of *Aspergillus fumigatus* in invasive aspergillosis. Clin Microbiol Rev **22:**447–465. http://dx.doi.org/10.1128/CMR.00055-08.
2. **Greenberger PA.** 2002. Allergic bronchopulmonary aspergillosis. J Allergy Clin Immunol **110:**685–692. http://dx.doi.org/10.1067/mai.2002.130179.
3. **Gibbons JG, Rokas A.** 2013. The function and evolution of the Aspergillus genome. Trends Microbiol **21:**14–22. http://dx.doi.org/10.1016/j.tim.2012.09.005.
4. **Kwon-Chung KJ, Sugui JA.** 2013. *Aspergillus fumigatus*—what makes the species a ubiquitous human fungal pathogen? PLoS Pathog **9:**e1003743. http://dx.doi.org/10.1371/journal.ppat.1003743.
5. **Perez-Nadales E, Nogueira MF, Baldin C, Castanheira S, El Ghalid M, Grund E, Lengeler K, Marchegiani E, Mehrotra PV, Moretti M, Naik V, Oses-Ruiz M, Oskarsson T, Schäfer K, Wasserstrom L, Brakhage AA, Gow NA, Kahmann R, Lebrun MH, Perez-Martin J, Di Pietro A, Talbot NJ, Toquin V, Walther A, Wendland J.** 2014. Fungal model systems and the elucidation of pathogenicity determinants. Fungal Genet Biol **70:**42–67. http://dx.doi.org/10.1016/j.fgb.2014.06.011.
6. **Shi Y.** 2009. Serine/threonine phosphatases: mechanism through structure. Cell **139:**468–484. http://dx.doi.org/10.1016/j.cell.2009.10.006.
7. **Pearson G, Robinson F, Gibson TB, Xu BE, Karandikar M, Berman K, Cobb MH.** 2001. Mitogen-activated protein (MAP) kinase pathways: regulation and physiological functions. Endocr Rev **22:**153–183. http://dx.doi.org/10.1210/edrv.22.2.0428.
8. **Heinisch JJ, Lorberg A, Schmitz HP, Jacoby JJ.** 1999. The protein kinase C-mediated MAP kinase pathway involved in the maintenance of cellular integrity in *Saccharomyces cerevisiae*. Mol Microbiol **32:**671–680. http://dx.doi.org/10.1046/j.1365-2958.1999.01375.x.
9. **Jung US, Levin DE.** 1999. Genome-wide analysis of gene expression regulated by the yeast cell wall integrity signaling pathway. Mol Microbiol **34:**1049–1057. http://dx.doi.org/10.1046/j.1365-2958.1999.01667.x.
10. **Bahn YS.** 2008. Master and commander in fungal pathogens: the two-component system and the HOG signaling pathway. Eukaryot Cell **7:**2017–2036. http://dx.doi.org/10.1128/EC.00323-08.
11. **Hamel LP, Nicole MC, Duplessis S, Ellis BE.** 2012. Mitogen-activated protein kinase signaling in plant-interacting fungi: distinct messages from conserved messengers. Plant Cell **24:**1327–1351. http://dx.doi.org/10.1105/tpc.112.096156.
12. **Monge RA, Román E, Nombela C, Pla J.** 2006. The MAP kinase signal transduction network in *Candida albicans*. Microbiology **152:**905–912. http://dx.doi.org/10.1099/mic.0.28616-0.
13. **Rispail N, Soanes DM, Ant C, Czajkowski R, Grünler A, Huguet R, Perez-Nadales E, Poli A, Sartorel E, Valiante V, Yang M, Beffa R, Brakhage AA, Gow NA, Kahmann R, Lebrun MH, Lenasi H, Perez-Martin J, Talbot NJ, Wendland J, Di Pietro A.** 2009.Comparative genomics of MAP kinase and calcium-calcineurin signalling components in plant and human pathogenic fungi. Fungal Genet Biol **46:**287–298. http://dx.doi.org/10.1016/j.fgb.2009.01.002.
14. **Román E, Arana DM, Nombela C, Alonso-Monge R, Pla J.** 2007. MAP kinase pathways as regulators of fungal virulence. Trends Microbiol **15:**181–190. http://dx.doi.org/10.1016/j.tim.2007.02.001.
15. **May GS, Xue T, Kontoyiannis DP, Gustin MC.** 2005. Mitogen activated protein kinases of *Aspergillus fumigatus*. Med Mycol **43**(Suppl 1)**:**S83–S86.
16. **May GS.** 2008. Mitogen-activated protein kinase pathways in aspergilli, p 121–127. *In* Goldman GH, Osmani SA (ed), The aspergilli. Genomics, medical aspects, biotechnology, and research methods. CRC Press, Boca Raton, FL.
17. **Reyes G, Romans A, Nguyen CK, May GS.** 2006. Novel mitogen-activated protein kinase MpkC of *Aspergillus fumigatus* is required for utilization of polyalcohol sugars. Eukaryot Cell **5:**1934–1940. http://dx.doi.org/10.1128/EC.00178-06.
18. **Valiante V, Heinekamp T, Jain R, Härtl A, Brakhage AA.** 2008. The mitogen-activated protein kinase MpkA of *Aspergillus fumigatus* regulates cell wall signaling and oxidative stress response. Fungal Genet Biol **45:**618–627. http://dx.doi.org/10.1016/j.fgb.2007.09.006.
19. **Valiante V, Jain R, Heinekamp T, Brakhage AA.** 2009. The MpkA MAP kinase module regulates cell wall integrity signaling and pyomelanin formation in *Aspergillus fumigatus*. Fungal Genet Biol **46:**909–918. http://dx.doi.org/10.1016/j.fgb.2009.08.005.
20. **Xue T, Nguyen CK, Romans A, May GS.** 2004. A mitogen-activated protein kinase that senses nitrogen regulates conidial germination and growth in *Aspergillus fumigatus*. Eukaryot Cell **3:**557–560. http://dx.doi.org/10.1128/EC.3.2.557-560.2004.
21. **Jain R, Valiante V, Remme N, Docimo T, Heinekamp T, Hertweck C, Gershenzon J, Haas H, Brakhage AA.** 2011. The MAP kinase MpkA controls cell wall integrity, oxidative stress response, gliotoxin production and iron adaptation in *Aspergillus fumigatus*. Mol Microbiol **82:**39–53. http://dx.doi.org/10.1111/j.1365-2958.2011.07778.x.
22. **Müller S, Baldin C, Groth M, Guthke R, Kniemeyer OO, Brakhage AA, Valiante V.** 2012. Comparison of transcriptome technologies in the pathogenic fungus *Aspergillus fumigatus* reveals novel insights into the genome and MpkA dependent gene expression. BMC Genomics **13:**519. http://dx.doi.org/10.1186/1471-2164-13-519.
23. **Dichtl K, Helmschrott C, Dirr F, Wagener JJ.** 2012. Deciphering cell wall integrity signalling in *Aspergillus fumigatus*: identification and functional characterization of cell wall stress sensors and relevant Rho GTPases. Mol Microbiol **83:**506–519. http://dx.doi.org/10.1111/j.1365-2958.2011.07946.x.
24. **Samantaray S, Neubauer M, Helmschrott C, Wagener J.** 2013. Role of the guanine nucleotide exchange factor Rom2 in cell wall integrity maintenance of *Aspergillus fumigatus*. Eukaryot Cell **12:**288–298. http://dx.doi.org/10.1128/EC.00246-12.
25. **Martín H, Flández M, Nombela C, Molina M.** 2005. Protein phosphatases in MAPK signalling: we keep learning from yeast. Mol Microbiol **58:**6–16. http://dx.doi.org/10.1111/j.1365-2958.2005.04822.x.
26. **Angeles de la Torre-Ruiz M, Torres J, Arino J, Herrero E.** 2002. Sit4 is required for proper modulation of the biological functions mediated by Pkc1 and the cell integrity pathway in *Saccharomyces cerevisiae*. J Biol Chem **277:**33468–33476. http://dx.doi.org/10.1074/jbc.M203515200.
27. **Huh WK, Falvo JV, Gerke LC, Carroll AS, Howson RW, Weissman JS, O'Shea EK.** 2003. Global analysis of protein localization in budding yeast. Nature **425:**686–691. http://dx.doi.org/10.1038/nature02026.
28. **Sutton A, Immanuel D, Arndt TK.** 1991. The SIT4 protein phosphatase functions in late G_1 for progression into S phase. Mol Cell Biol **11:**2133–2148.
29. **Zabrocki P, Van Hoof C, Goris J, Thevelein JM, Winderickx J, Wera S.** 2002. Protein phosphatase 2A on track for nutrient-induced signalling in yeast. Mol Microbiol **43:**835–842. http://dx.doi.org/10.1046/j.1365-2958.2002.02786.x.
30. **Jacinto E.** 2007. Phosphatase targets in TOR signaling. Methods Mol Biol **365:**323–334.
31. **Winkelströter LK, Bom VLP, de Castro PA, Ramalho LNZ, Goldman MHS, Brown NA, Rajendran R, Ramage G, Bovier E, Dos Reis TF, Savoldi M, Hagiwara D, Goldman GH.** 2015. High osmolarity glycerol response (HOG) PtcB phosphatase is important for *Aspergillus fumigatus* virulence. Mol Microbiol **96:**42–54. http://dx.doi.org/10.1111/mmi.12919.
32. **Kafer E.** 1977. Meiotic and mitotic recombination in *Aspergilllus* and its chromosomal aberrations. Adv Genet **19:**33–131.
33. **Colot HH, Park G, Turner GE, Ringelberg C, Crew CM, Litvinkova L, Weiss RL, Borkovich KA, Dunlap JC.** 2006. A high-throughput gene knockout procedure for *Neurospora* reveals functions for multiple tran-

scription factors. Proc Natl Acad Sci U S A **103:**10352–10357. http://dx.doi.org/10.1073/pnas.0601456103.
34. **Schiestl RH, Gietz RD.** 1989. High efficiency transformation of intact yeast cells using single stranded nucleic acids as a carrier. Curr Genet **16:**339–346. http://dx.doi.org/10.1007/BF00340712.
35. **Sambrook J, Fritsch EF, Maniatis T.** 1989. Molecular cloning: a laboratory manual. Cold Spring Harbor Laboratory, Cold Spring Harbor, NY.
36. **Mowat E, Butcher J, Lang S, Williams C, Ramage G.** 2007. Development of a simple model for studying the effects of antifungal agents on multicellular communities of *Aspergillus fumigatus*. J Med Microbiol **56:**1205–1212. http://dx.doi.org/10.1099/jmm.0.47247-0.
37. **Shopova I, Bruns S, Thywissen A, Kniemeyerm O, Brakhage AA, Hillmann F.** 2013. Extrinsic extracellular DNA leads to biofilm formation and colocalizes with matrix polysaccharides in the human pathogenic fungus *Aspergillus fumigatus*. Front Microbiol **4:**141. http://dx.doi.org/10.3389/fmicb.2013.00141.
38. **Erlandsen SL, Kristich CJ, Dunny GM, Wells CL.** 2004. High-resolution visualization of the microbial glycocalyx with low-voltage scanning electron microscopy: dependence on cationic dyes. J Histochem Cytochem **52:**1427–1435. http://dx.doi.org/10.1369/jhc.4A6428.2004.
39. **Walker LA, Munro CA, de Bruijn I, Lenardon MD, McKinnon A, Gow NA.** 2008. Stimulation of chitin synthesis rescues *Candida albicans* from echinocandins. PLoS Pathog **4:**e1000040. http://dx.doi.org/10.1371/journal.ppat.1000040.
40. **Shepardson KM, Ngo LY, Aimanianda V, Latge JP, Barker BM, Blosser SJ, Iwakura Y, Hohl TM, Cramer RA.** 2013. Hypoxia enhances innate immune activation to *Aspergillus fumigatus* through cell wall modulation. Microbes Infect **15:**259–269. http://dx.doi.org/10.1016/j.micinf.2012.11.010.
41. **Graham LM, Tsoni SV, Willment JA, Williams DL, Taylor PR, Gordon S, Dennehy K, Brown GD.** 2006. Soluble Dectin-1 as a tool to detect beta-glucans. J Immunol Methods **314:**164–169. http://dx.doi.org/10.1016/j.jim.2006.05.013.
42. **Beauvais A, Bozza S, Kniemeyer O, Formosa C, Balloy V, Henry C, Roberson RW, Dague E, Chignard M, Brakhage AA, Romani L, Latgé JP.** 2013. Deletion of the alpha-(1,3)-glucan synthase genes induces a restructuring of the conidial cell wall responsible for the avirulence of *Aspergillus fumigatus*. PLoS Pathog **9:**e1003716. http://dx.doi.org/10.1371/journal.ppat.1003716.
43. **Rauch A, Bellew M, Eng J, Fitzgibbon M, Holzman T, Hussey P, Igra M, Maclean B, Lin CW, Detter A, Fang R, Faca V, Gafken P, Zhang H, Whiteaker J, States D, Hanash S, Paulovich A, McIntosh MW.** 2006. Computational Proteomics Analysis System (CPAS): an extensible, open-source analytic system for evaluating and publishing proteomic data and high throughput biological experiments. J Proteome Res **5:**112–121. http://dx.doi.org/10.1021/pr0503533.
44. **Dinamarco TM, Almeida RS, de Castro PA, Brown NA, dos Reis TF, Ramalho LN, Savoldi M, Goldman MH, Goldman GH.** 2012. Molecular characterization of the putative transcription factor SebA involved in virulence in *Aspergillus fumigatus*. Eukaryot Cell **11:**518–531. http://dx.doi.org/10.1128/EC.00016-12.
45. **Mech F, Thywissen FA, Guthke R, Brakhage AA, Figge MT.** 2011. Automated image analysis of the host-pathogen interaction between phagocytes and *Aspergillus fumigatus*. PLoS One **6:**e19591. http://dx.doi.org/10.1371/journal.pone.0019591.
46. **Marim FM, Silveira TN, Lima DS, Jr, Zamboni DS.** 2010. A method for generation of bone marrow-derived macrophages from cryopreserved mouse bone marrow cells. PLoS One **5:**e15263. http://dx.doi.org/10.1371/journal.pone.0015263.
47. **Yamaguchi H, Uchida K, Nagino K, Matsunaga T.** 2002. Usefulness of a colorimetric method for testing antifungal drug susceptibilities of Aspergillus species to voriconazole. J Infect Chemother **8:**374–377. http://dx.doi.org/10.1007/s10156-002-0201-Y.
48. **Bradford MM.** 1976. A rapid and sensitive method for the quantitation of microgram quantities of protein utilizing the principle of protein-dye binding. Anal Biochem **72:**248–254. http://dx.doi.org/10.1016/0003-2697(76)90527-3.
49. **Hagiwara D, Takahashi-Nakaguchi A, Toyotome T, Yoshimi A, Abe K, Kamei K, Gonoi T, Kawamoto S.** 2013. NikA/TcsC histidine kinase is involved in conidiation, hyphal morphology, and responses to osmotic stress and antifungal chemicals in *Aspergillus fumigatus*. PLoS One **8:**e80881. http://dx.doi.org/10.1371/journal.pone.0080881.
50. **Stark MJ.** 1996. Yeast protein serine/threonine phosphatases: multiple roles and diverse regulation. Yeast **12:**1647–1675.
51. **Herbert JM, Augereau JM, Gleye J, Maffrand JP.** 1990. Chelerythrine is a potent and specific inhibitor of protein kinase C. Biochem Biophys Res Commun **172:**993–999. http://dx.doi.org/10.1016/0006-291X(90)91544-3.
52. **Arpaia G, Cerri F, Baima S, Macino G.** 1999. Involvement of protein kinase C in the response of *Neurospora crassa* to blue light. Mol Gen Genet **262:**314–322. http://dx.doi.org/10.1007/s004380051089.
53. **Jarvis WD, Grant S.** 1999. Protein kinase C targeting in antineoplastic treatment strategies. Invest New Drugs **17:**227–240. http://dx.doi.org/10.1023/A:1006328303451.
54. **da Rocha AB, Mans DR, Regner A, Schwartsmann G.** 2002. Targeting protein kinase C: new therapeutic opportunities against high-grade malignant gliomas? Oncologist **7:**17–33. http://dx.doi.org/10.1634/theoncologist.7-1-17.
55. **Sussman A, Hus K, Chio LC, Heidler S, Shaw M, Ma D, Zhu Z, Campbell RM, Park TS, Kulanthaivel P, Scott JE, Carpenter JW, Strege MA, Belvo MD, Swartling JR, Fischl A, Yeh WK, Shih C, Ye XS.** 2004. Discovery of cercosporamide, a known antifungal natural product, as a selective Pkc1 kinase inhibitor through high-throughput screening. Eukaryot Cell **3:**932–943. http://dx.doi.org/10.1128/EC.3.4.932-943.2004.
56. **Juvvadi PR, Maruyama J, Kitamoto K.** 2007. Phosphorylation of the *Aspergillus oryzae* Woronin body protein, AoHex1, by protein kinase C: evidence for its role in the multimerization and proper localization of the Woronin body protein. Biochem J **405:**533–540. http://dx.doi.org/10.1042/BJ20061678.
57. **Philippe B, Ibrahim-Granet O, Prévost MC, Gougerot-Pocidalo MA, Sanchez Perez M, Van der Meeren A, Latgé JP.** 2003. Killing of *Aspergillus fumigatus* by alveolar macrophages is mediated by reactive oxidant intermediates. Infect Immun **71:**3034–3042. http://dx.doi.org/10.1128/IAI.71.6.3034-3042.2003.
58. **Mehrad B, Strieter RM, Standiford TJ.** 1999. Role of TNF-alpha in pulmonary host defense in murine invasive aspergillosis. J Immunol **162:**1633–1640.
59. **Taramelli D, Malabarba MG, Sala G, Basilico N, Cocuzza G.** 1996. Production of cytokines by alveolar and peritoneal macrophages stimulated by *Aspergillus fumigatus* conidia or hyphae. J Med Vet Mycol **34:**49–56. http://dx.doi.org/10.1080/02681219680000081.
60. **Jiang Y, Broach JR.** 1999. Tor proteins and protein phosphatase 2A reciprocally regulate Tap42 in controlling cell growth in yeast. EMBO J **18:**2782–2792. http://dx.doi.org/10.1093/emboj/18.10.2782.
61. **Yu F, Gu Q, Yun Y, Yin Y, Xu JR, Shim WB, Ma Z.** 2014. The TOR signaling pathway regulates vegetative development and virulence in *Fusarium graminearum*. New Phytol **203:**219–232. http://dx.doi.org/10.1111/nph.12776.
62. **Di Como CJ, Arndt KT.** 1996. Nutrients, via the Tor proteins, stimulate the association of Tap42 with type 2A phosphatases. Genes Dev **10:**1904–1916. http://dx.doi.org/10.1101/gad.10.15.1904.
63. **Beck T, Hall MN.** 1999. The TOR signalling pathway controls nuclear localization of nutrient-regulated transcription factors. Nature **402:**689–692. http://dx.doi.org/10.1038/45287.
64. **Masuda CA, Ramírez J, Peña A, Montero-Lomelí M.** 2000. Regulation of monovalent ion homeostasis and pH by the Ser-Thr protein phosphatase SIT4 in *Saccharomyces cerevisiae*. J Biol Chem **275:**30957–30961. http://dx.doi.org/10.1074/jbc.M004869200.
65. **Mann DJ, Dombrádi V, Cohen PT.** 1993. *Drosophila* protein phosphatase V functionally complements a SIT4 mutant in *Saccharomyces cerevisiae* and its amino-terminal region can confer this complementation to a heterologous phosphatase catalytic domain. EMBO J **12:**4833–4842.
66. **Hayashi N, Nomura T, Sakumoto N, Mukai Y, Kaneko Y, Harashima S, Murakami S.** 2005. The SIT4 gene, which encodes protein phosphatase 2A, is required for telomere function in *Saccharomyces cerevisiae*. Curr Genet **47:**359–367. http://dx.doi.org/10.1007/s00294-005-0577-1.
67. **Montero-Lomeli M, Morais BLB, Figueiredo DL, Neto DCS, Martins JRP, Masuda CA.** 2002. The initiation factor eIF4A is involved in the response to lithium stress in *Saccharomyces cerevisiae*. J Biol Chem **277:**21542–21548. http://dx.doi.org/10.1074/jbc.M201977200.
68. **Lee CM, Nantel A, Jiang L, Whiteway M, Shen SH.** 2004. The serine/threonine protein phosphatase SIT4 modulates yeast-to-hypha morphogenesis and virulence in *Candida albicans*. Mol Microbiol **51:**691–709. http://dx.doi.org/10.1111/j.1365-2958.2003.03879.x.
69. **Sellam A, Mvan het Hoog Tebbji F, Beaurepaire C, Whiteway M, Nantel A.** 2014. Modeling the transcriptional regulatory network that

controls the early hypoxic response in *Candida albicans*. Eukaryot Cell **13:**675–690. http://dx.doi.org/10.1128/EC.00292-13.

70. **Aimanianda V, Bayry J, Bozza S, Kniemeyer O, Perruccio K, Elluru SR, Clavaud C, Paris S, Brakhage AA, Kaveri SV, Romani L, Latgé JP.** 2009. Surface hydrophobin prevents immune recognition of airborne fungal spores. Nature **460:**1117–1121. http://dx.doi.org/10.1038/nature08264.
71. **Aimanianda V, Latgé JP.** 2010. Fungal hydrophobins form a sheath preventing immune recognition of airborne conidia. Virulence **1:**185–187. http://dx.doi.org/10.4161/viru.1.3.11317.
72. **Carrion SDJ, Leal SM, Jr, Ghannoum MA, Aimanianda V, Latgé JP, Pearlman E.** 2013. The RodA hydrophobin on *Aspergillus fumigatus* spores masks dectin-1- and dectin-2-dependent responses and enhances fungal survival in vivo. J Immunol **191:**2581–2588. http://dx.doi.org/10.4049/jimmunol.1300748.
73. **Levin DE.** 2005. Cell wall integrity signaling in *Saccharomyces cerevisiae*. Microbiol Mol Biol Rev **69:**262–291. http://dx.doi.org/10.1128/MMBR.69.2.262-291.2005.
74. **Faro-Trindade I, Willment JA, Kerrigan AM, Redelinghuys P, Hadebe S, Reid DM, Srinivasan N, Wainwright H, Lang DM, Steele C, Brown GD.** 2012. Characterisation of innate fungal recognition in the lung. PLoS One **7:**e35675. http://dx.doi.org/10.1371/journal.pone.0035675.
75. **Hohl TM, Van Epps HL, Rivera A, Morgan LA, Chen PL, Feldmesser M, Pamer EGEG.** 2005. *Aspergillus fumigatus* triggers inflammatory responses by stage specific beta-glucan display. PLoS Pathog **1:**e30. http://dx.doi.org/10.1371/journal.ppat.0010030.
76. **Huang H, Ostroff GR, Lee CK, Wang JP, Specht CA, Levitz SM.** 2009. Distinct patterns of dendritic cell cytokine release stimulated by fungal beta-glucans and Toll-like receptor agonists. Infect Immun **77:**1774–1781. http://dx.doi.org/10.1128/IAI.00086-09.
77. **Steele C, Rapaka RR, Metz A, Pop SM, Williams DL, Gordon S, Kolls JK, Brown GD.** 2005. The beta-glucan receptor dectin-1 recognizes specific morphologies of *Aspergillus fumigatus*. PLoS Pathog **1:**e42. http://dx.doi.org/10.1371/journal.ppat.0010042.